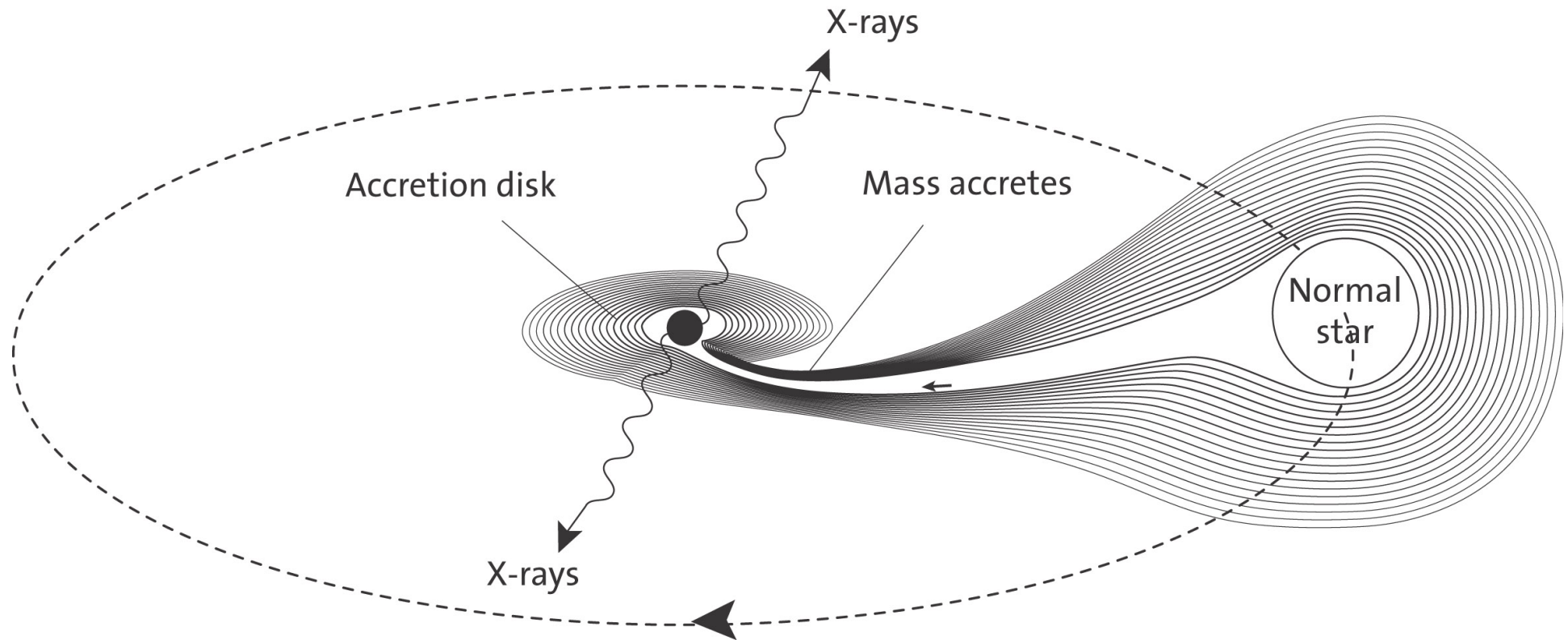


Astrofisica Nucleare e Subnucleare

“X-ray” Astrophysics

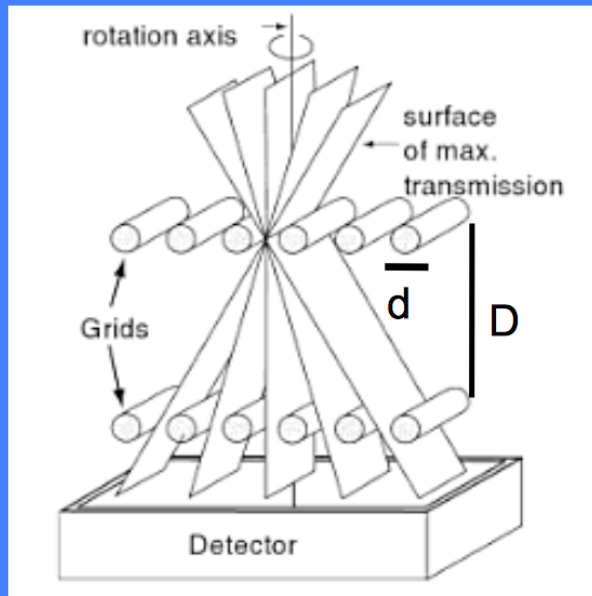
Nobel prize 2002 – R.Giacconi



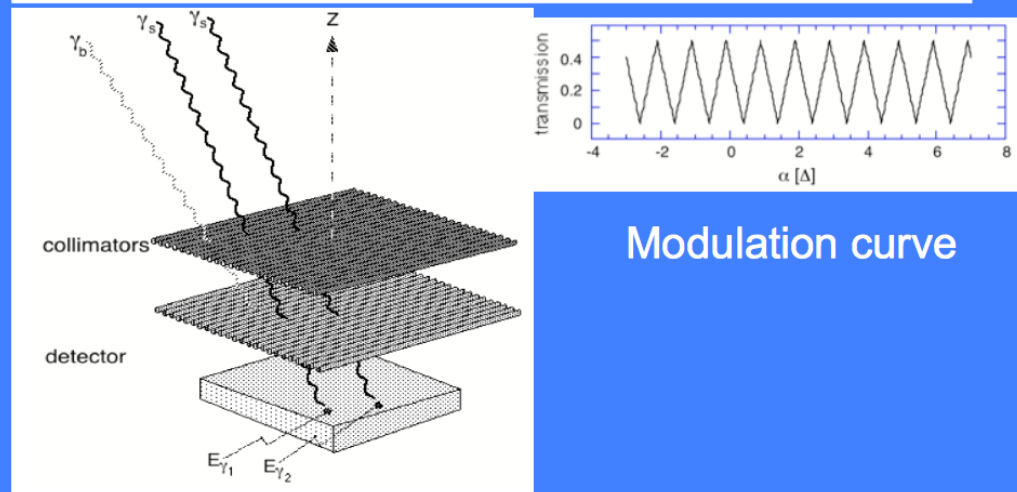
“ ... for pioneering contributions to astrophysics,
which have led to the discovery of cosmic X-ray sources”

Scanning Grid Collimators

- Two or more plane (“grid” of absorbing rods) collimators to improve angular resolution
- Higher resolution with three or more grids (e.g., 4 in HEAO-1 A-3 experiment)
- Two-dimensional measurements need scans in two or more directions



Double-grid collimator
Transmission Function of triangular shape
Angular resolution: d/D



Modulation curve

$$C_B = B A_d \Delta E \Delta t$$

Background counts from a collimated telescope with detector area A_d , sensitive over the band ΔE , in a time interval Δt

$$\sigma(C_B) = C_B^{1/2}$$

The counts obey the Poisson statistics

$$C_S = S_E A_d \Delta E \Delta t \eta_E$$

Source counts collected from a source with flux S_E in the same conditions ($QE = \eta_E$)

$$C_{\text{meas}} = (C_S + C_B) - C_B$$

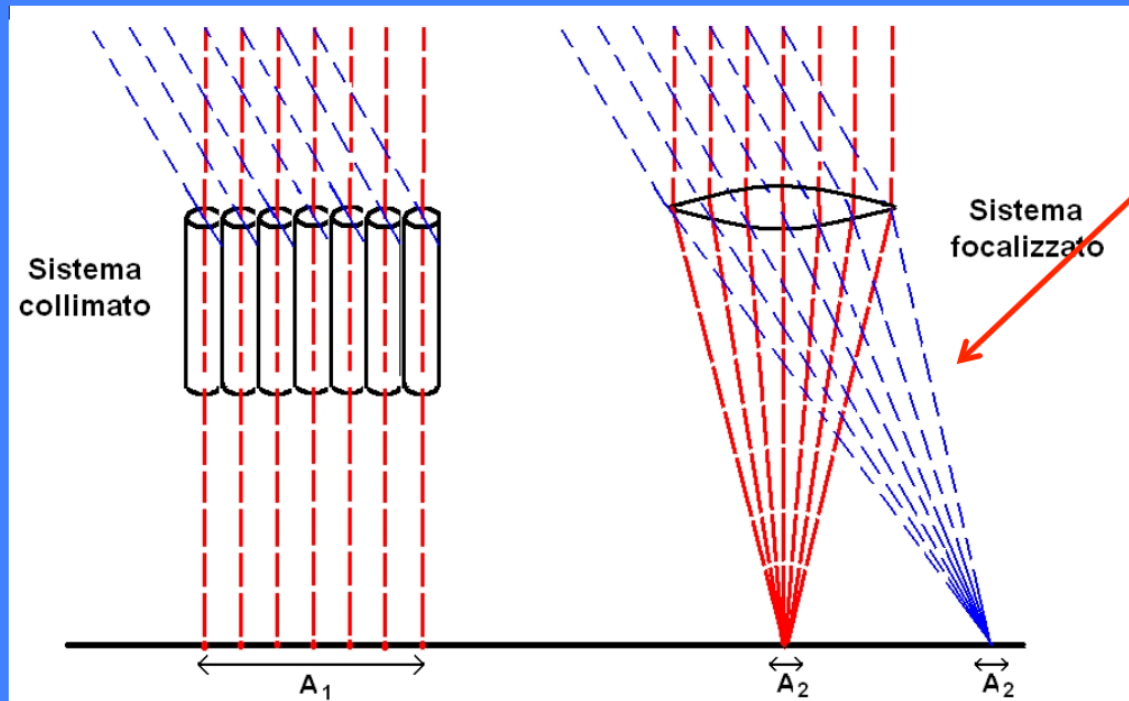
Measured counts (backg-subtracted)

$$\sigma^2(C_{\text{meas}}) = 2\sigma^2(C_B)$$

Background dominates fluctuations

$$S/N = n_\sigma = \frac{C_S}{\sqrt{2C_B}} = \frac{S_E A_d \Delta E \Delta t \eta_E}{\sqrt{2B A_d \Delta E \Delta t}}$$
$$S_{E,\text{min}} = \frac{n_\sigma}{\eta_E} \frac{\sqrt{2B}}{\sqrt{A_d \Delta t \Delta E}}$$

Focalizzazione vs collimazione



Proper imaging of X-rays below 20-40 keV

A_d = PSF projected on the focal plane

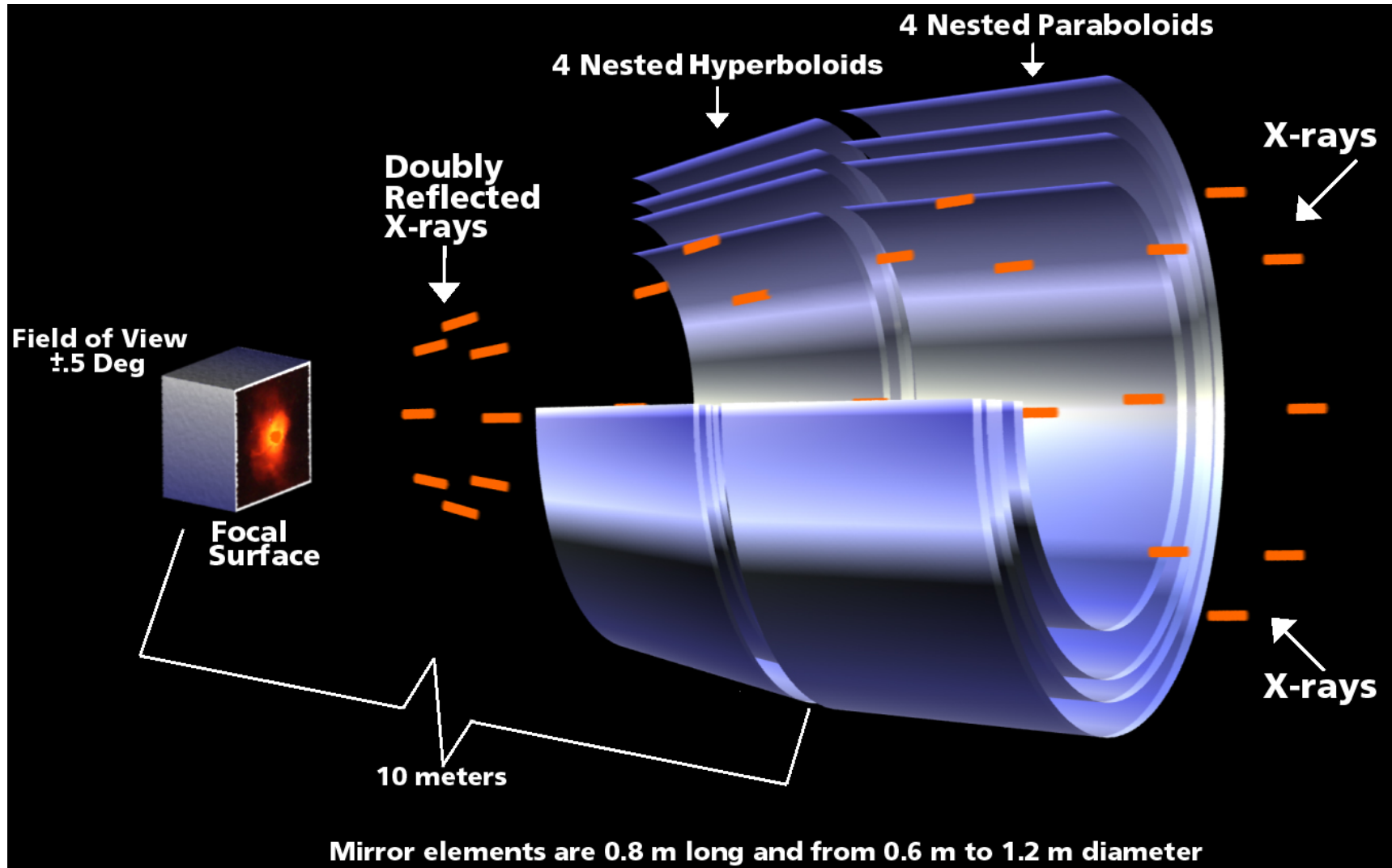
$$F_{\min} \approx n_{\sigma} \frac{\sqrt{2B}}{\sqrt{A_{\text{det}} T_{\text{int}} \Delta E}}$$

$$F_{\min} \approx n_{\sigma} \frac{\sqrt{BA_d}}{A_{\text{eff}} \sqrt{T_{\text{int}} \Delta E}}$$

Sistema collimato: limita la regione di cielo da cui puo' provenire un segnale, (quindi limita il background), non incrementandone la "densita"

Sistema focalizzato: fa corrispondere ad ogni sorgente un punto nel piano focale, e "concentra" il segnale, producendo un'immagine

X-Ray Mirrors



Why do we use X-ray optics

- To achieve the best 2-dim angular resolution
 - To distinguish nearby sources or different regions of the same source
 - To perform morphological studies
- As a collector to “gather” weak fluxes (case of limited photon statistics)
- As a concentrator, so that the image photons may interact in a small region of the detector, thus limiting the influence of the background
- To serve with high spectral resolution dispersive spectrometers such as transmission or reflection gratings
- To simultaneously measure both the source(s) of interest and the contaminating background in other (source-free) regions of the detector

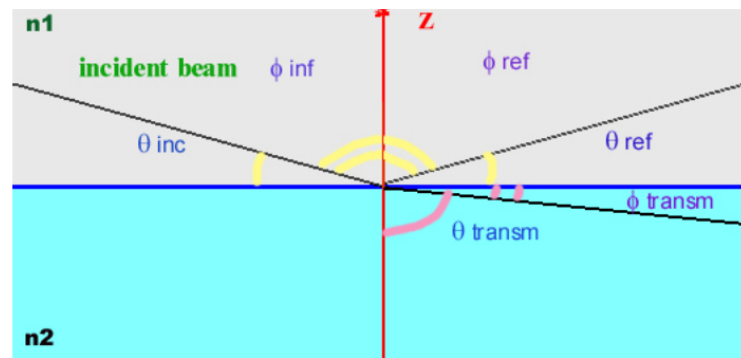
X-ray optical constants

- X-rays are hard to refract or reflect: the refractive index of all materials in X-rays is very close to 1 and only slightly less than 1 → X-rays are above the characteristic energy of bonded e⁻ in atoms
- complex index of refraction of the reflector to describe the interaction X-rays /matter (see, for a review, Aschembach et al. 1985, Rep. Prog. Phys. 48, 579)

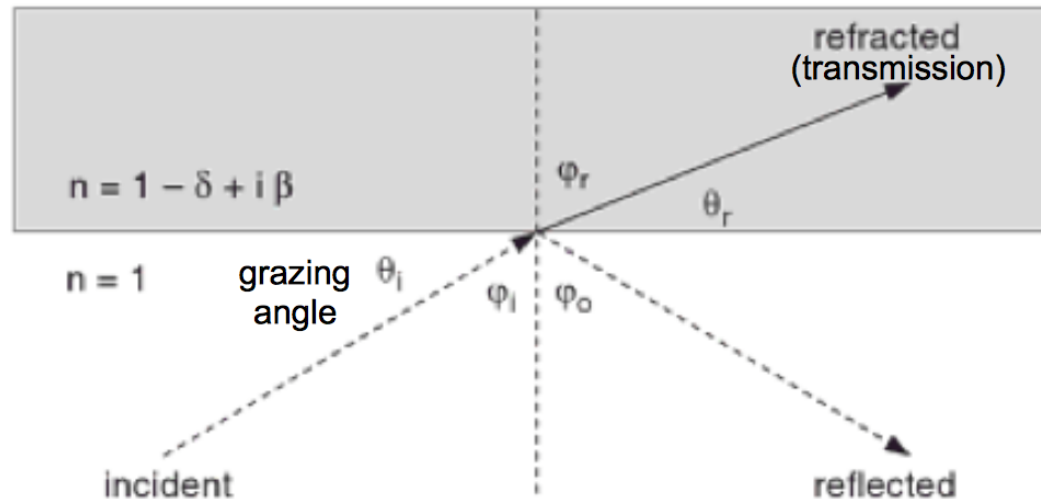
$$n=1-\delta+i\beta$$

where δ describes the phase change and
 β accounts for the absorption

δ and β depend on the wavelength



- the amplitude of reflection is described by the Fresnel's equations



$$n_1 = 1, n_2 = (1 - \delta) \rightarrow \sin \phi_i = (1 - \delta) \sin \phi_r$$

$$\vartheta = (\pi / 2) - \phi$$

$$\cos(90 - \phi_i) = \cos \vartheta_i = (1 - \delta) \cos(90 - \phi_r) = (1 - \delta) \cos \vartheta_r$$

$$\Rightarrow \cos \vartheta_i = \cos \vartheta_r (1 - \delta)$$

Total reflection if no real solution for ϑ_r
 $\delta > 0, \cos \theta_r \leq 1 \rightarrow$ There is a **critical angle** θ_c below which refraction is impossible
 and total external reflection occurs (grazing angle, $\theta_i = \theta_c$)



Extreme case for
low θ_r values

$$1 = \cos \vartheta_r = \cos \vartheta_c / (1 - \delta) \rightarrow \cos \vartheta_c = 1 - \delta$$

Total X-ray reflection at grazing incidence

- Real part of n slightly less than unity for matter at X-rays, =1 in vacuum (total external reflection); $\delta \ll 1$

- Snell's law ($n_1 \cos\theta_1 = n_2 \cos\theta_2$) to find a critical angle for total reflection

- (Total) external reflection in vacuum for angles $<$ critical angle: $\cos\theta_{crit} = 1 - \delta$

- X-ray partially reflected also for $\theta > \theta_{crit}$; also, some absorption in the material

- $\cos(\theta_{crit}) = 1 - \theta_{crit}^2/2 = 1 - \delta \xrightarrow{\text{low angles}} \theta_{crit} = \sqrt{2\delta}$

- Far from fluorescent edges:

$$\delta \approx \frac{N_0 Z r_e \rho \lambda^2}{2\pi A}$$

where N_0 =Avogadro's number

Z =atomic number

r_e =electron radius

ρ =density

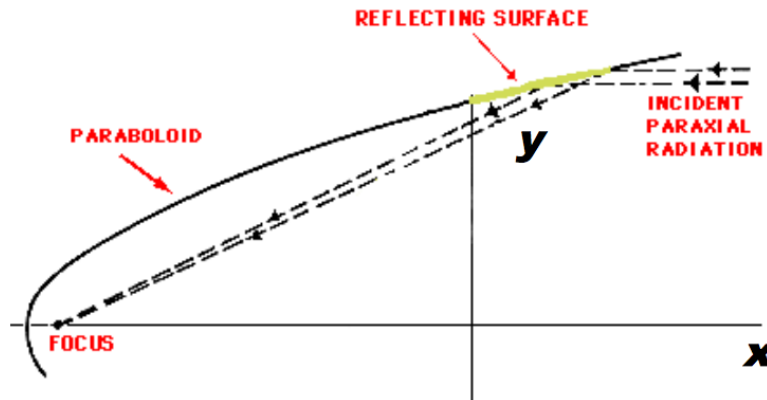
λ =wavelength of the incoming photon

A =atomic weight

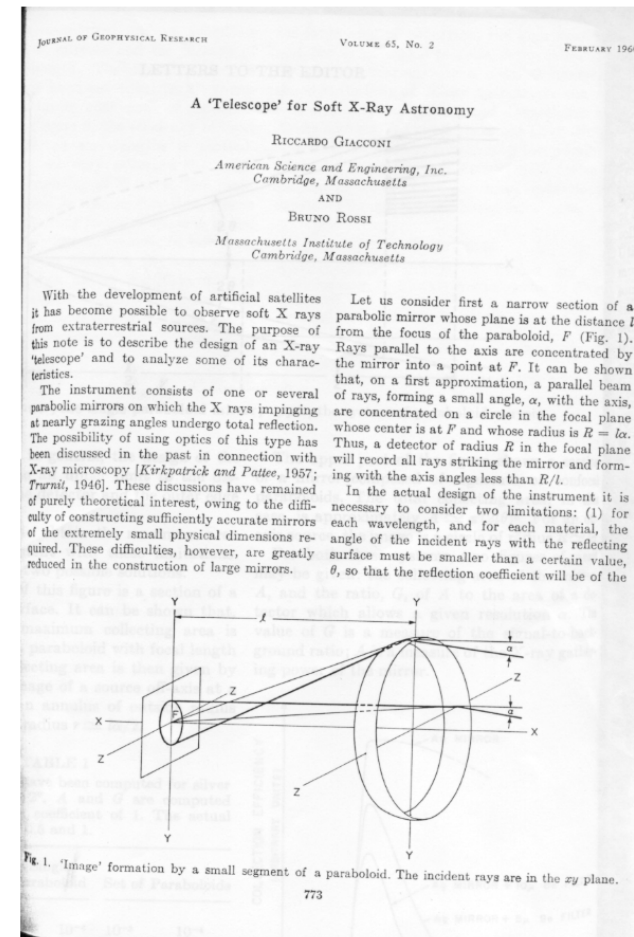
Critical angle:

- Inversely dependent on energy
- Higher Z materials reflect higher energies, for a fixed grazing angle
- Higher Z materials have a larger critical angle at any energy

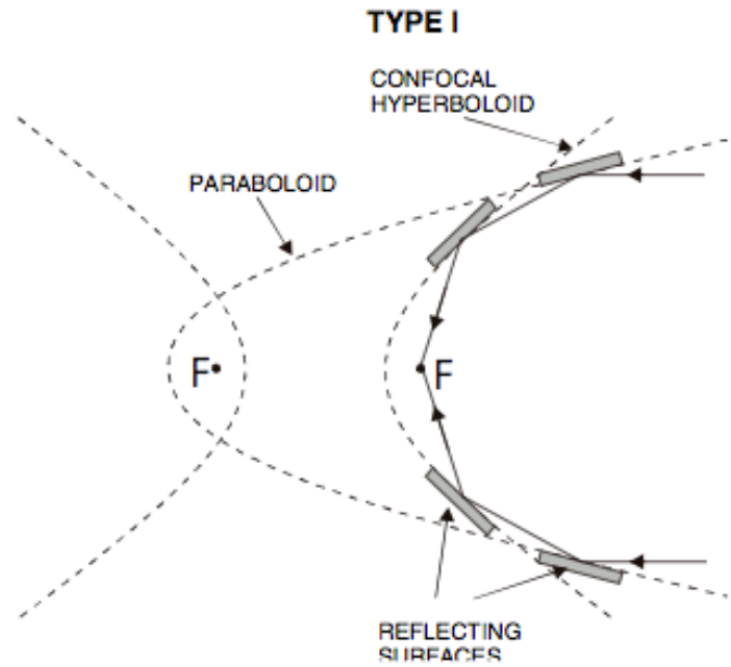
X-ray mirrors with parabolic profile



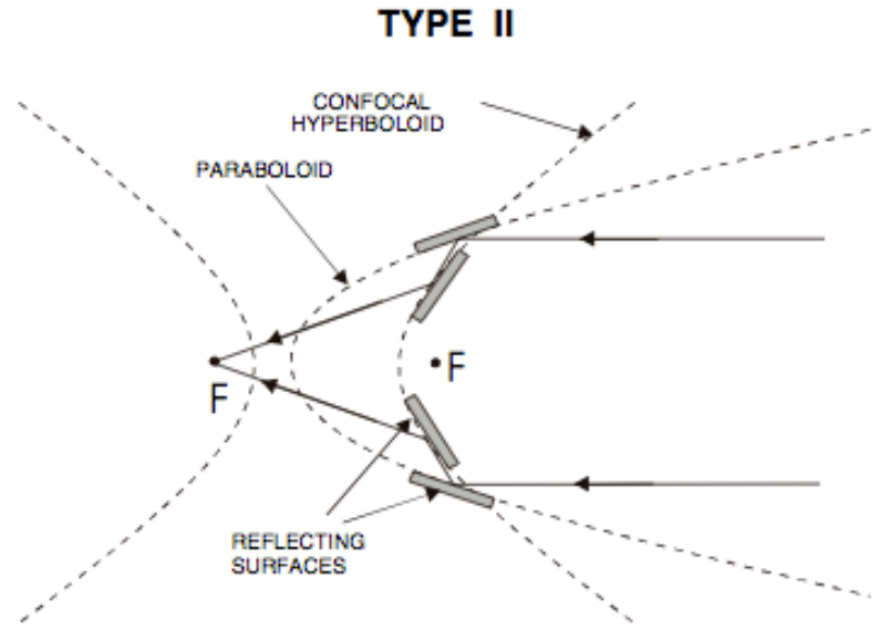
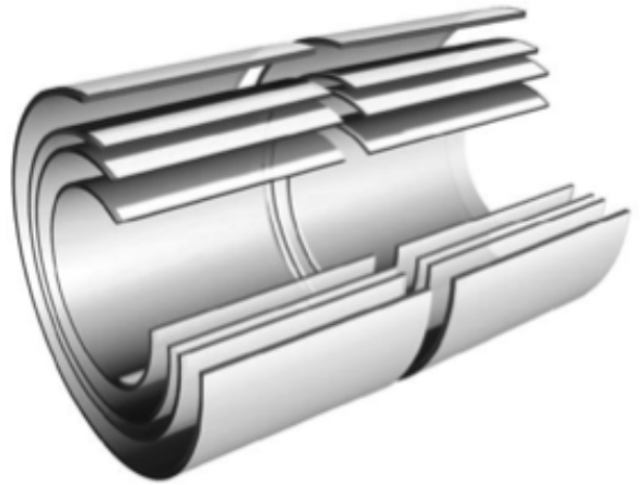
- perfect on-axis focusing
- off-axis images strongly affected by coma



Wolter, 1952

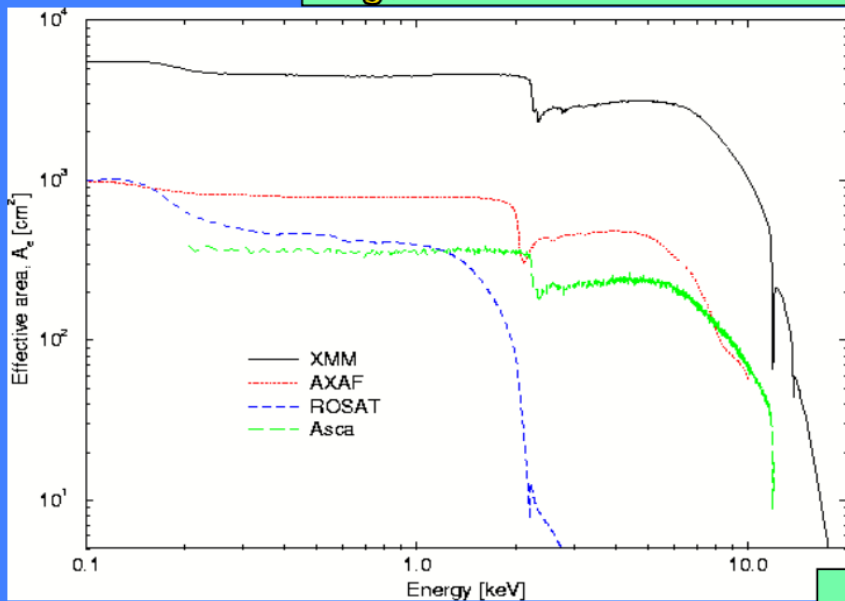


Wolter-I optics
 Paraboloid → Hyperboloid

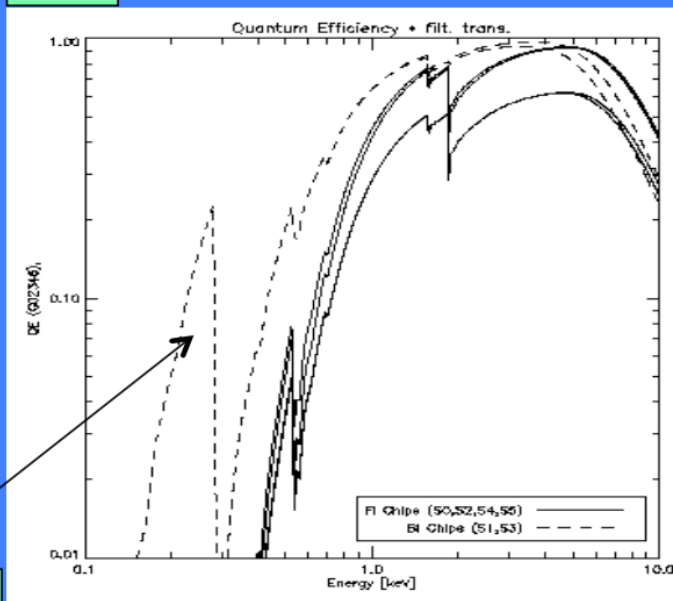


Wolter-II optics
 Paraboloid → Hyperboloid (ext. surface)

$A_{\text{geom}} \times \text{Reflectivity}$

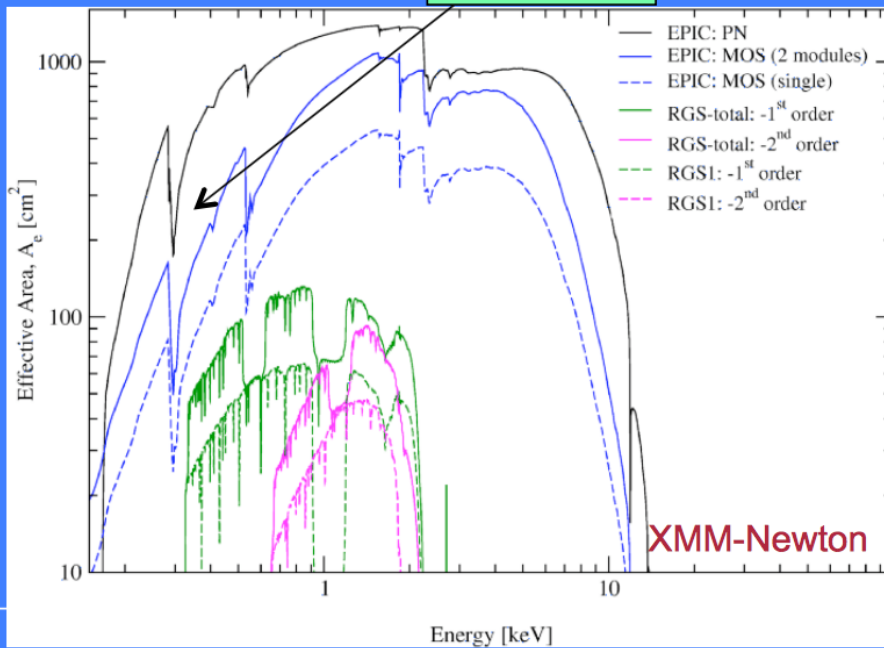


QE



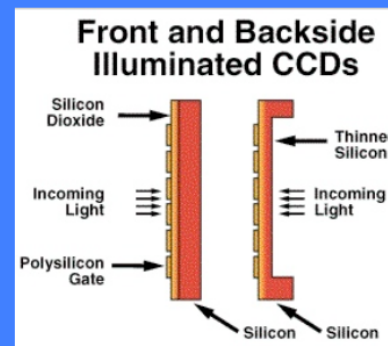
\times

$A_{\text{effective}}$



$=$

CCD



$$C_S = S_E A_e \Delta E \Delta t \eta_E$$

Detected signal

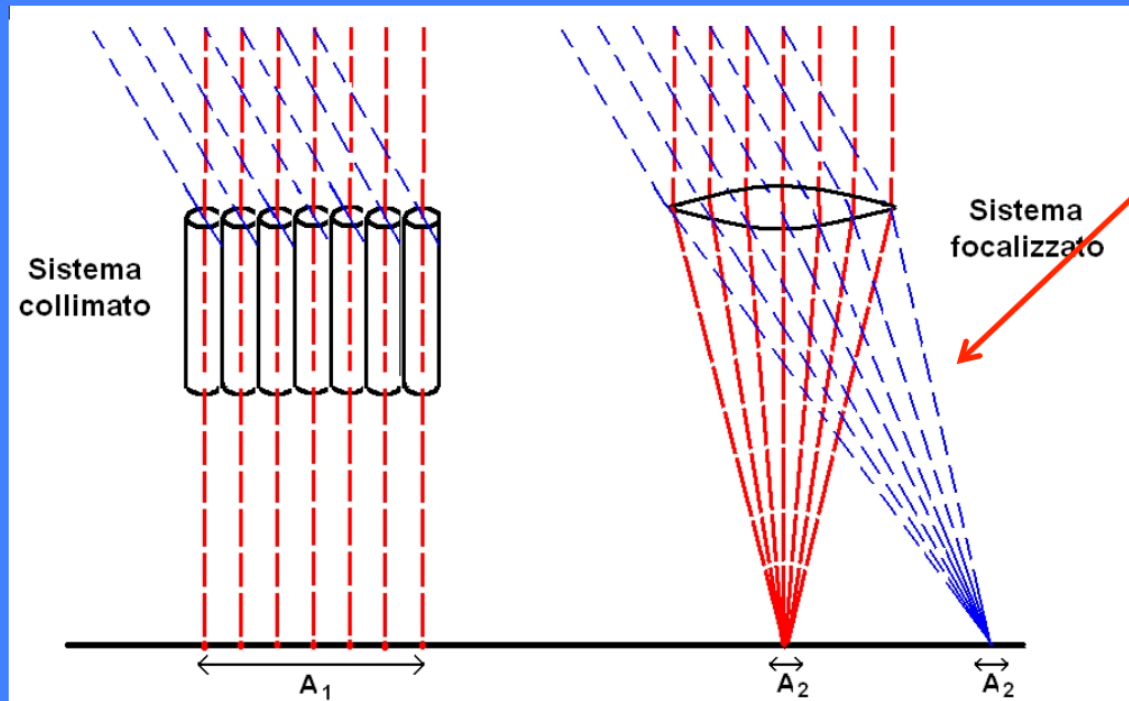
$$C_B = B \varepsilon A_d \Delta E \Delta t$$

Background signal (ε : region of the detector where B counts are focused)

$$S/N = n_\sigma = \frac{C_S}{\sqrt{C_S + 2C_B}} \approx \frac{S_E A_e \Delta E \Delta t \eta_E}{\sqrt{2B \varepsilon A_d \Delta E \Delta t}}$$
$$S_{E,\min} = \frac{n_\sigma}{\eta_E} \frac{1}{A_e} \sqrt{\frac{2B \varepsilon A_d}{\Delta t \Delta E}}$$

Weak sources

Focalizzazione vs collimazione



Proper imaging of X-rays below 20-40 keV

A_d = PSF projected on the focal plane

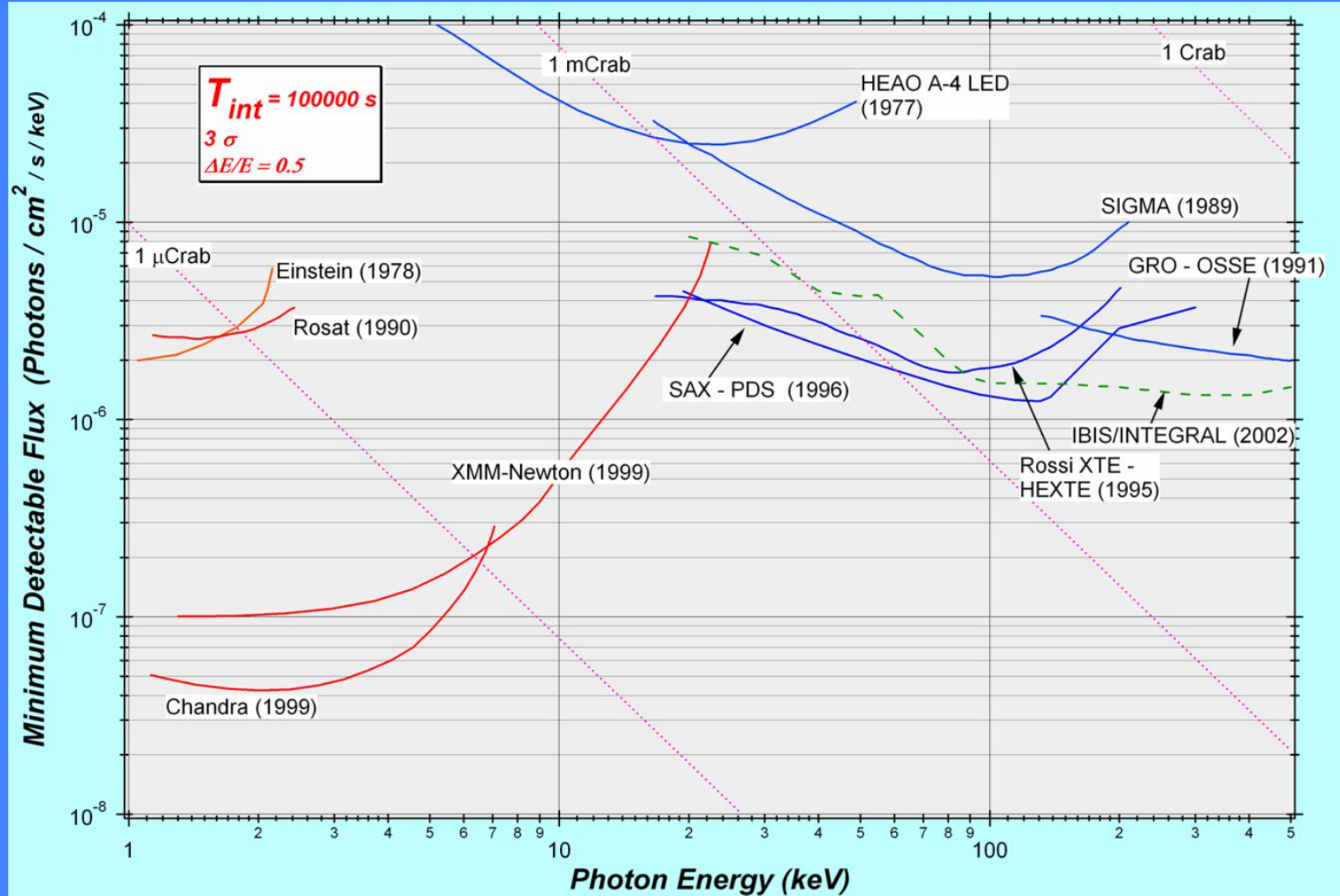
$$F_{\min} \approx n_{\sigma} \frac{\sqrt{2B}}{\sqrt{A_{\text{det}} T_{\text{int}} \Delta E}}$$

$$F_{\min} \approx n_{\sigma} \frac{\sqrt{BA_d}}{A_{\text{eff}} \sqrt{T_{\text{int}} \Delta E}}$$

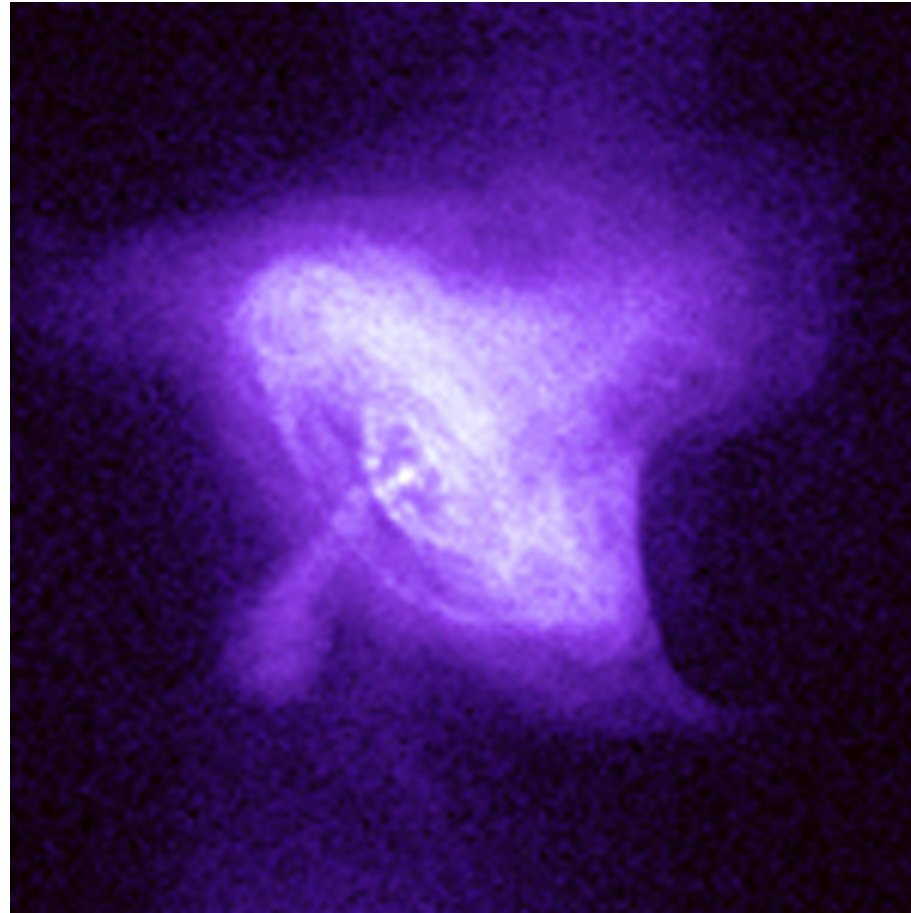
Sistema collimato: limita la regione di cielo da cui puo' provenire un segnale, (quindi limita il background), non incrementandone la "densita"

Sistema focalizzato: fa corrispondere ad ogni sorgente un punto nel piano focale, e "concentra" il segnale, producendo un'immagine

Old slide but *Chandra* and *XMM-Newton* still working

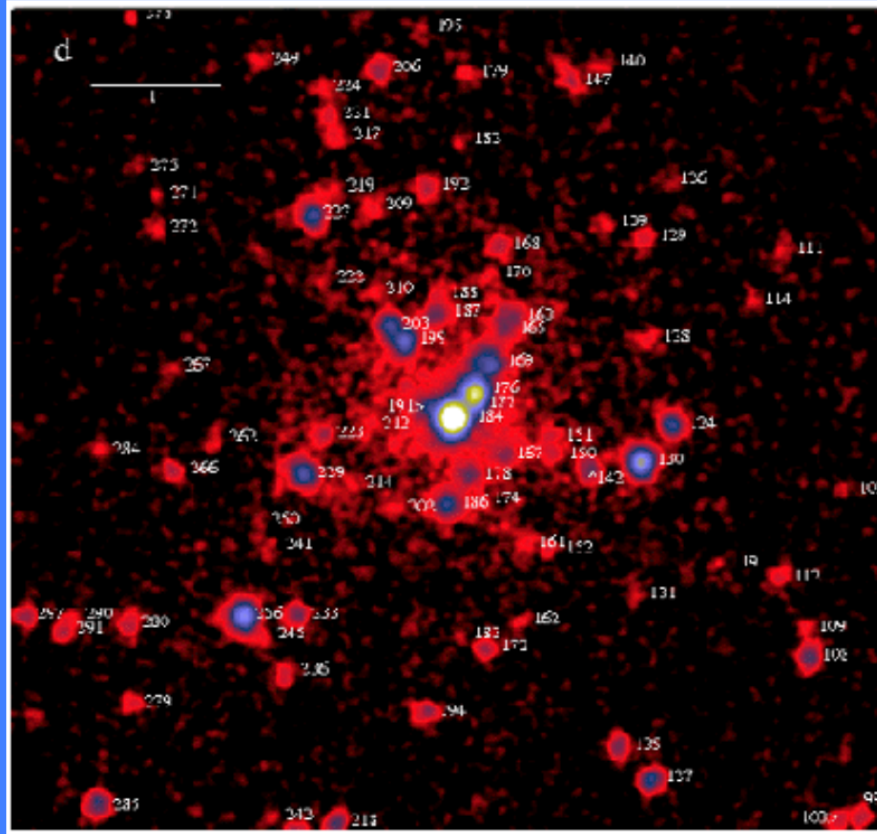


X-ray imaging

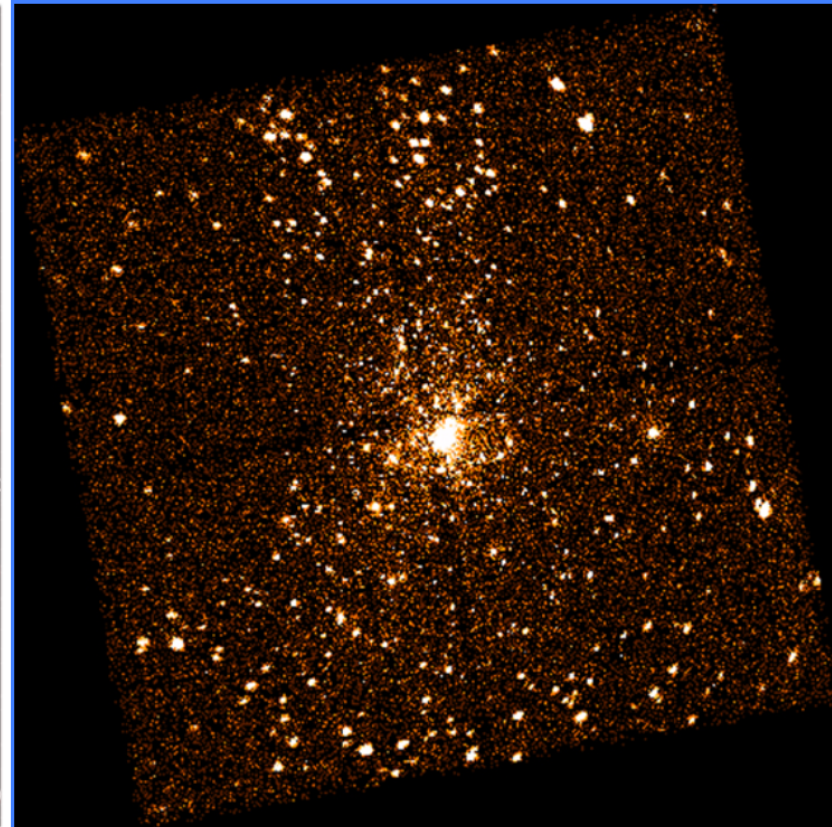


Crab nebula, 2.5", 0.3 – 3 keV

La risoluzione angolare in astronomia X: da *ROSAT* a *Chandra*

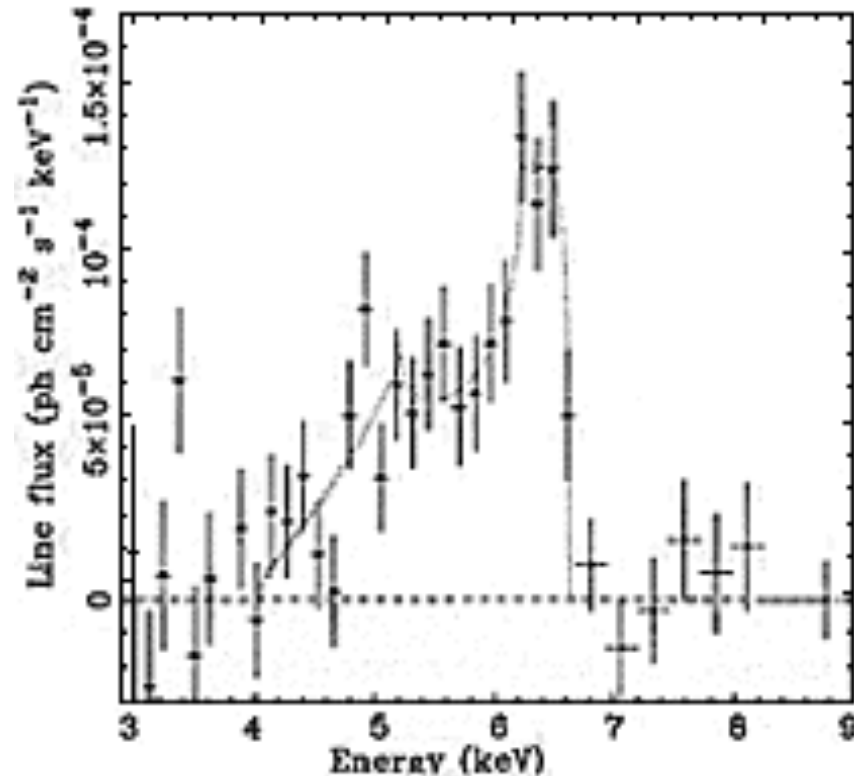


Osservazione di Orion
con ROSAT HRI (47 ks)



Osservazione di Orion
con Chandra ACIS (13.7 ks)

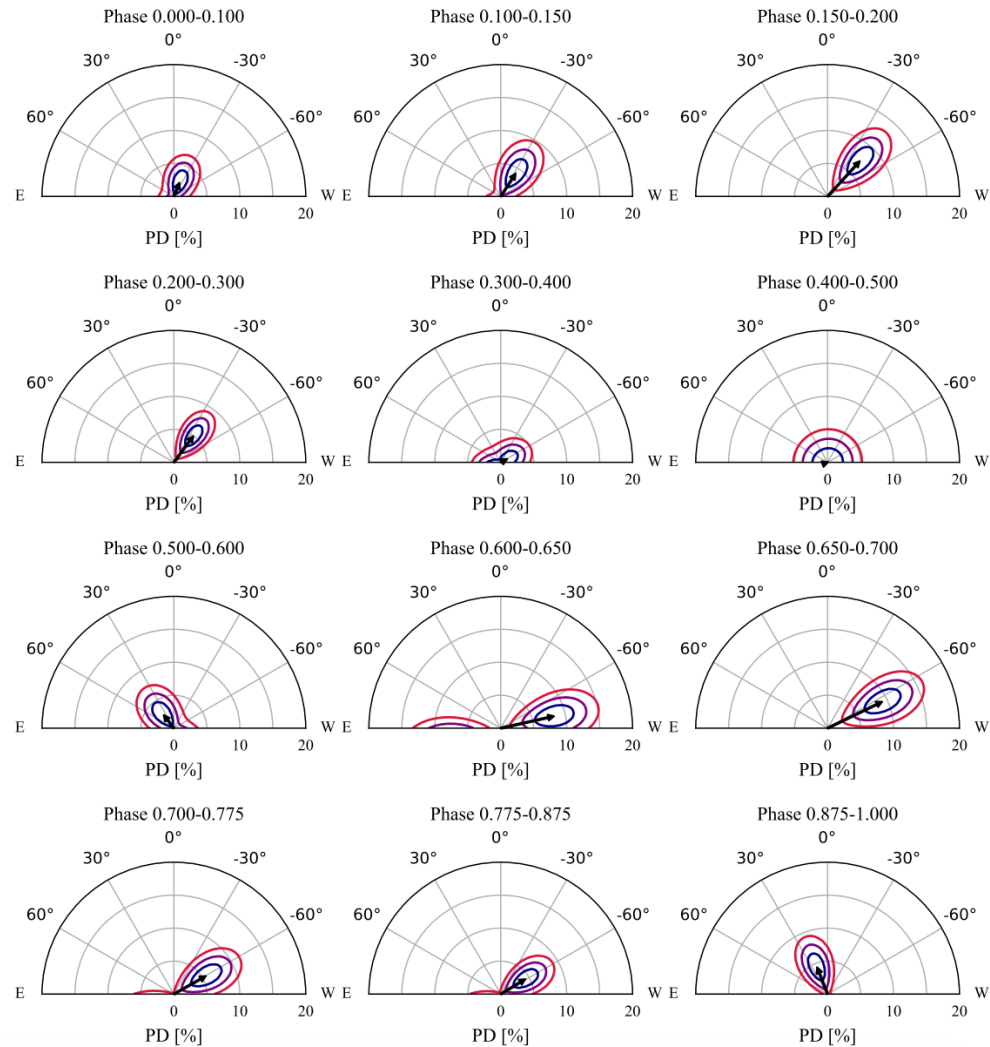
X-ray spectroscopy



The Fe line profile of K-alpha in the X-ray emission from the active nucleus of the galaxy MCG 6-30-15 in the constellation Centaurus is powered by matter accreting into a black hole. 19

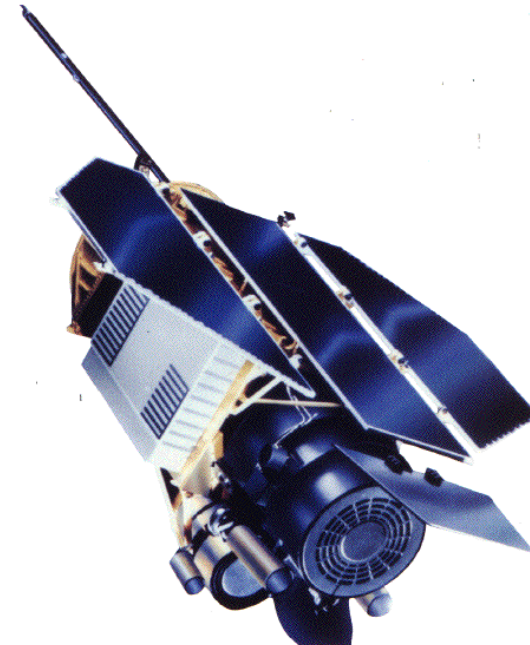
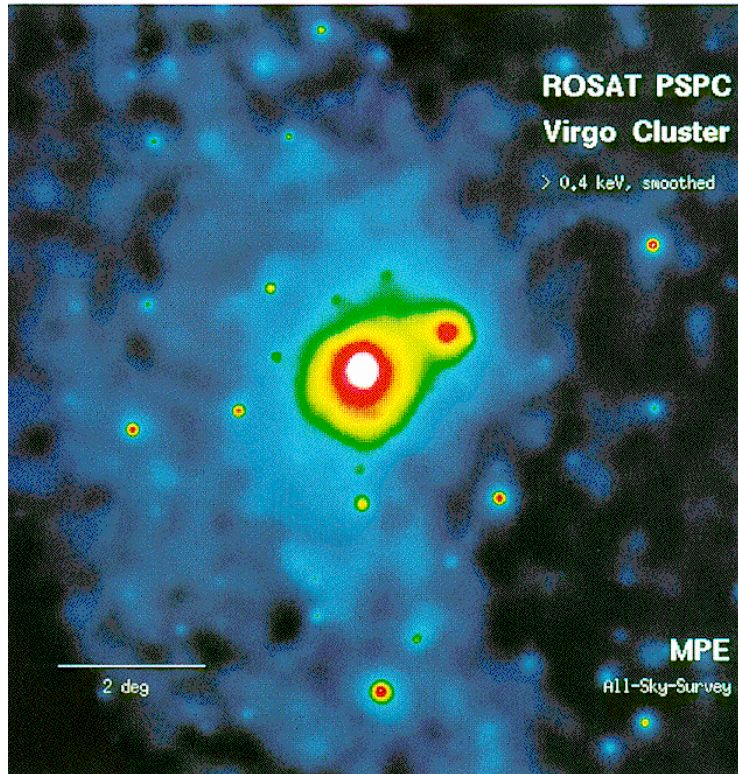
X-ray polarimetry

Polarization vectors of Vela X-1 from the results of the phase-resolved spectro-polarimetric analysis of the combined data set.



ROSAT

<http://www.mpe.mpg.de/xray/wave/rosat/>



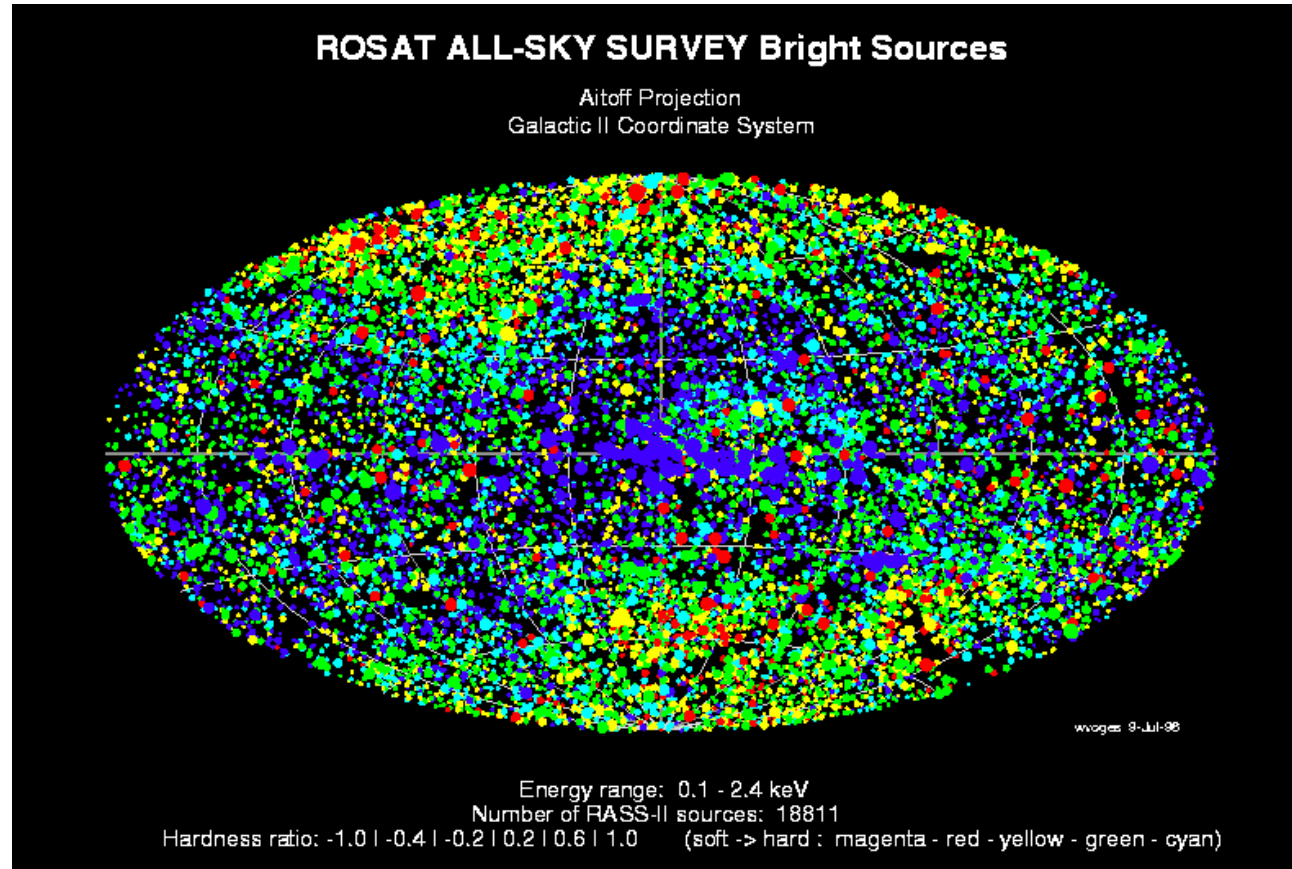
The scientific payload consists two coalligned scientific experiments, the [The X-Ray Telescope](#) which is used in conjunction with one of the focal plane instruments:

- [The Position Sensitive Proportional Counter](#)
- [The High Resolution Imager](#)

and the [The Wide Field Camera](#) which has its own mirror system and star sensor.

ROSAT provides a ~ 2 degree diameter field of view with the PSPC in the focal plane, and ~ 40 arcmin diameter field of view with the HRI in the focal plane. The ROSAT mission began with a six-month, all-sky PSPC survey, after which the satellite began a series of pointed observations that continued for the duration of the project.

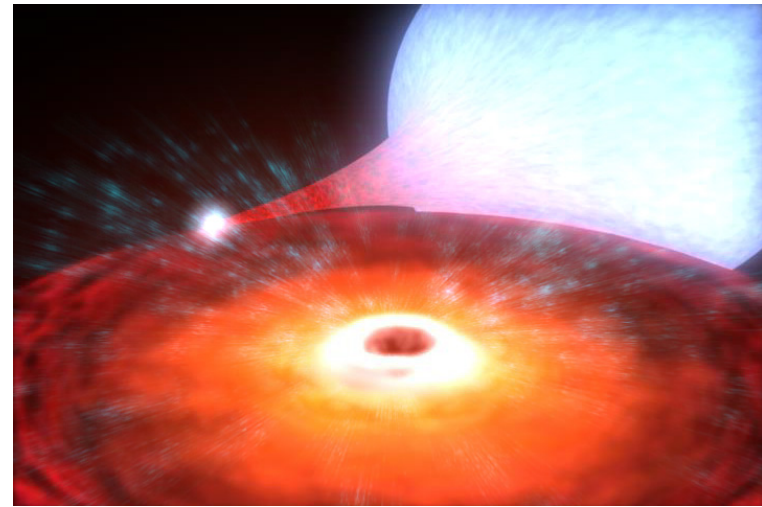
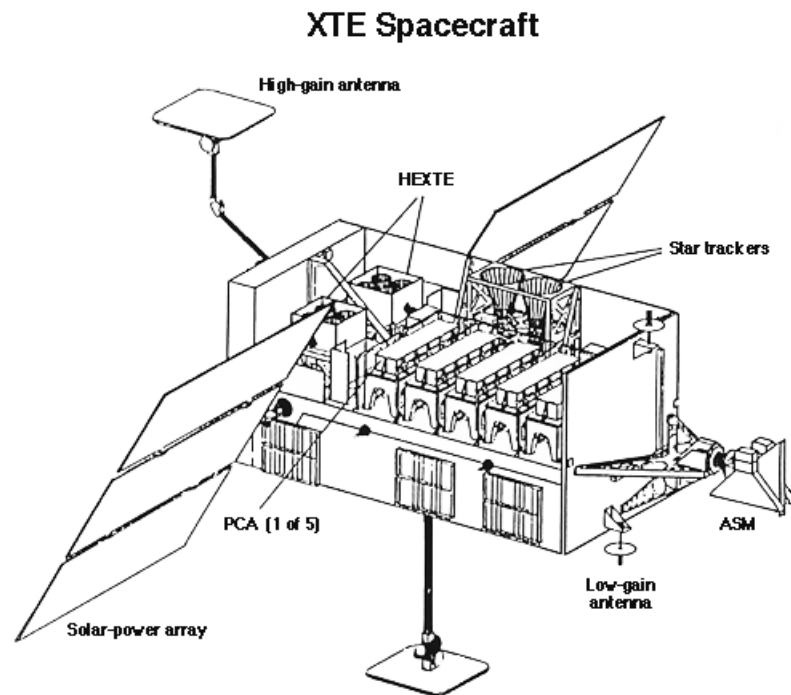
ROSAT results



The ROSAT All-Sky Survey Bright Source Catalogue (RASS-BSC, revision 1RXS) is derived from the all-sky survey performed during the first half year of the ROSAT mission in 1990/91. 18,811 sources are catalogued, with a limiting ROSAT PSPC countrate of 0.05 cts/s in the 0.1-2.4 keV energy band. 22

RXTE

<http://heasarc.gsfc.nasa.gov/docs/xte/xtegif.html>

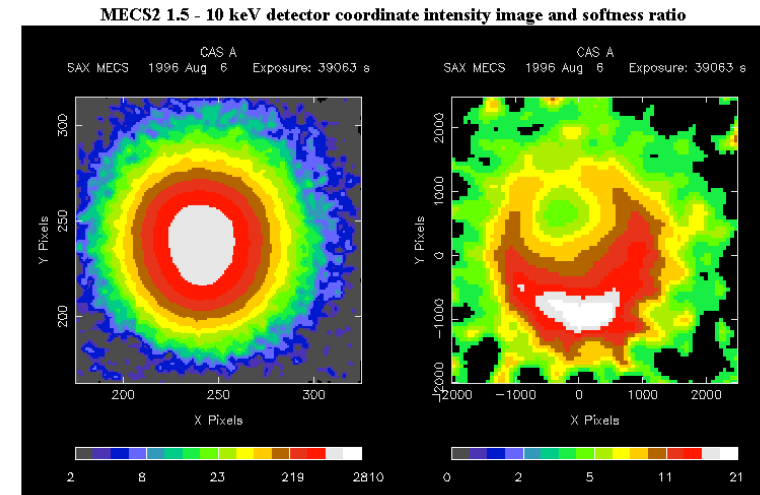
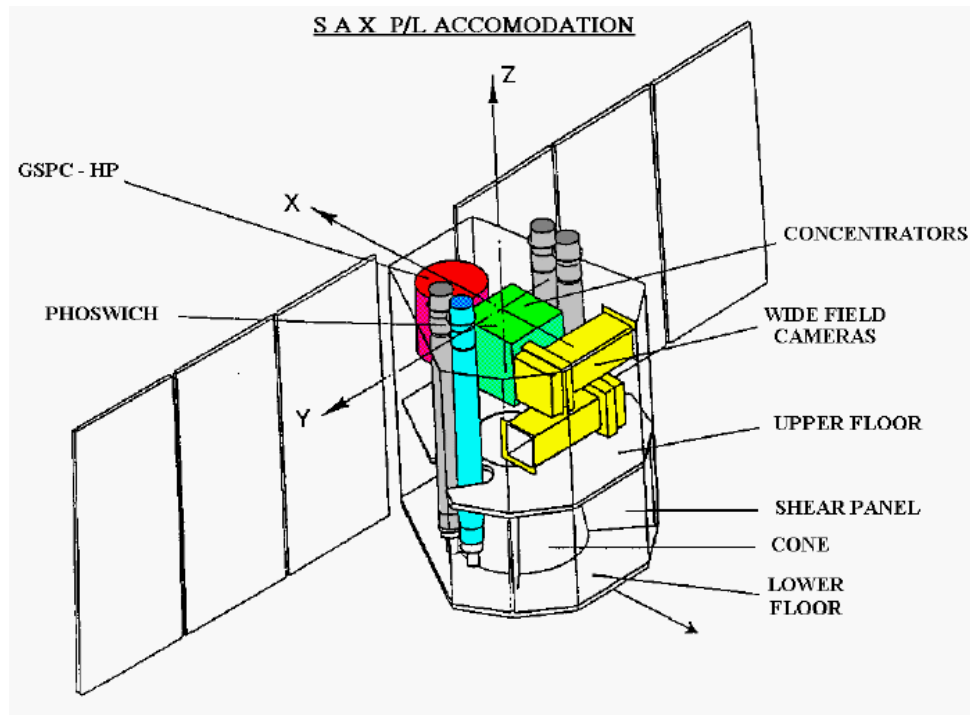


The lowest-mass known black hole belongs to a binary system named XTE J1650-500. The black hole has about 3.8 times the mass of our sun, and is orbited by a companion star

The Rossi X-ray Timing Explorer (RXTE) was launched on December 30, 1995. RXTE features unprecedented time resolution in combination with moderate spectral resolution to explore the variability of X-ray sources. Time scales from microseconds to months are covered in an instantaneous spectral range from 2 to 250 keV. Originally designed for a required lifetime of two years with a goal of five, it operated up to 2012

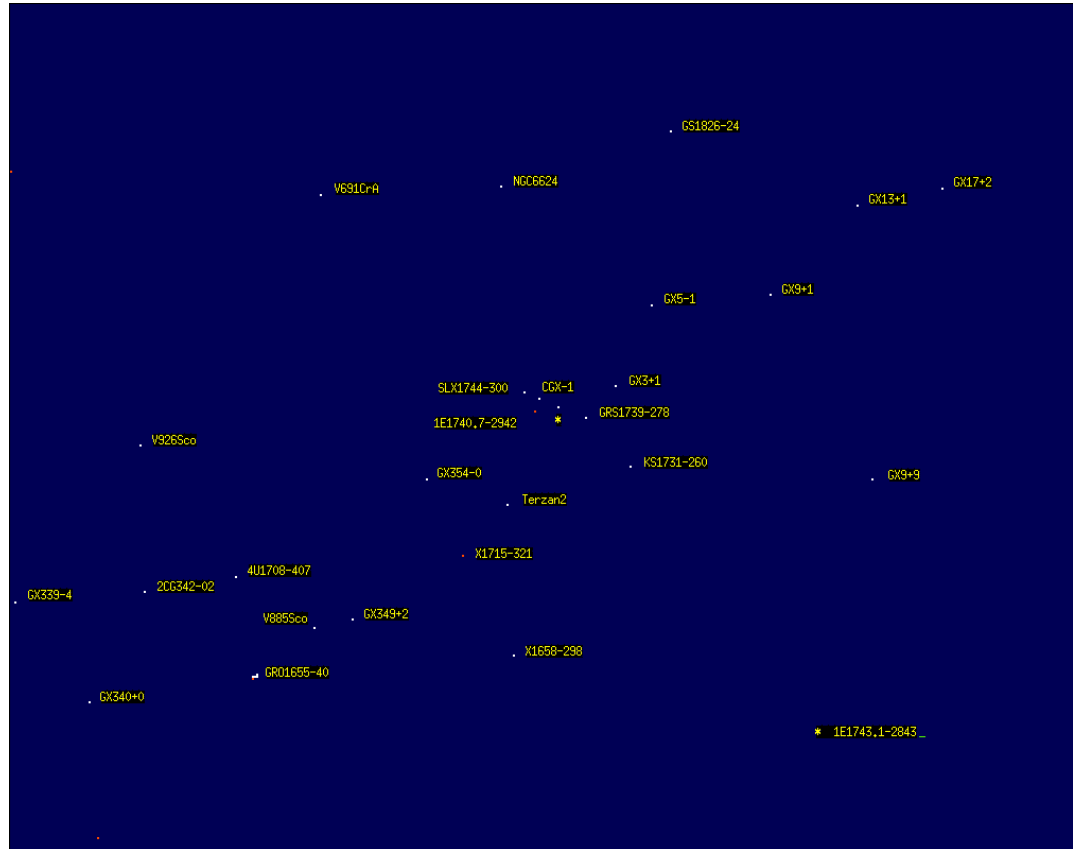
BeppoSAX

<http://www.asdc.asi.it/bepposax>



- Energy Range 0.1 to 200 keV
- Imaging capabilities (1') in the range of 0.1-10 keV.
- High energy (3-300 keV)
- Narrow fields and point in the same direction (Narrow Field Instruments, NFI).
- Monitoring large regions of the sky with a resolution of 5' in the range 2-30 keV
 - two coded mask proportional counters pointing in diametrically opposed directions perpendicular to the NFI
- Anticoincidence scintillator shields of the PDS will be used as a gamma-ray burst monitor in the range 60-600 keV.

BeppoSAX results

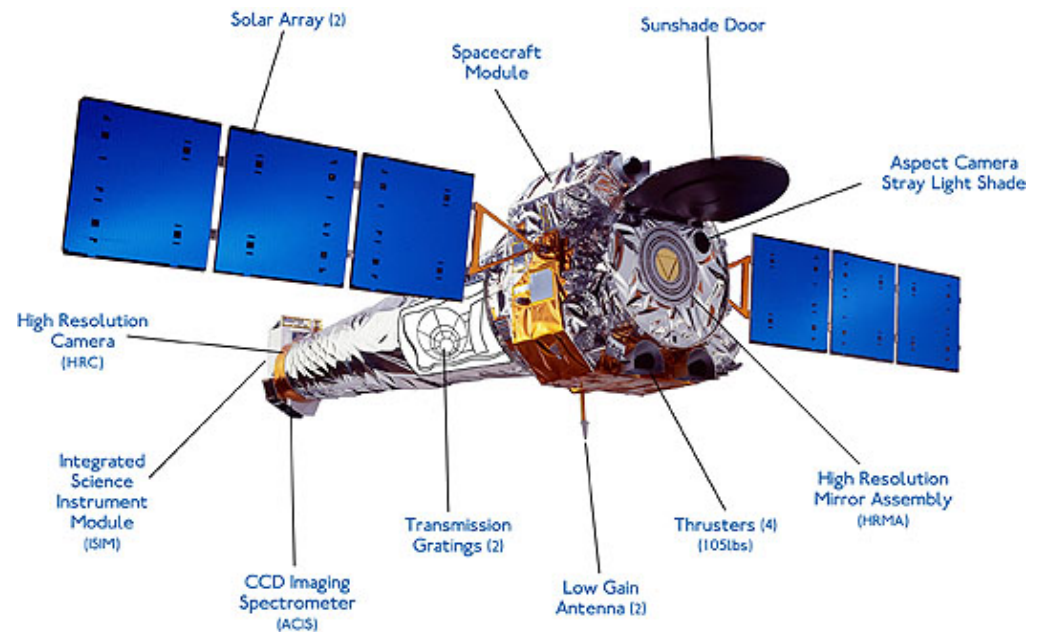


The Galactic Centre has been observed with the Beppo SAX Wide Field Camera 1 (WFC1) in August 1996. Here an image is shown of the 40 degrees by 40. The observation period was from 22-8-1996 07.54 UT through to 23-8-1996 11.38 UT, while the effective exposure totalled about 51 kiloseconds. The number of accepted events was 1.7955×10^7 in the energy range of 5.4 - 11.3 keV. The legenda for the galactic centre source indicated with a yellow star (1E1743.1-2843), is given at lower right in the image.

To our knowledge this is the largest field ever imaged in X-rays in a single pointing.

Chandra X-ray Telescope

<http://chandra.harvard.edu/>



High resolution mirror
two imaging detectors
two sets of transmission gratings.
Spatial resolution: 0.5"
Good sensitivity from 0.1 to 10 keV
High spectral resolution $E/\Delta E = 1000$ 26

XMM-Newton

<http://sci.esa.int/xmm-newton/>



XMM carries the X-ray telescopes with the largest effective area.

58 thin nested mirror shells in each X-ray telescope.

Moderate and high spectral resolution.

Simultaneous optical/UV observations

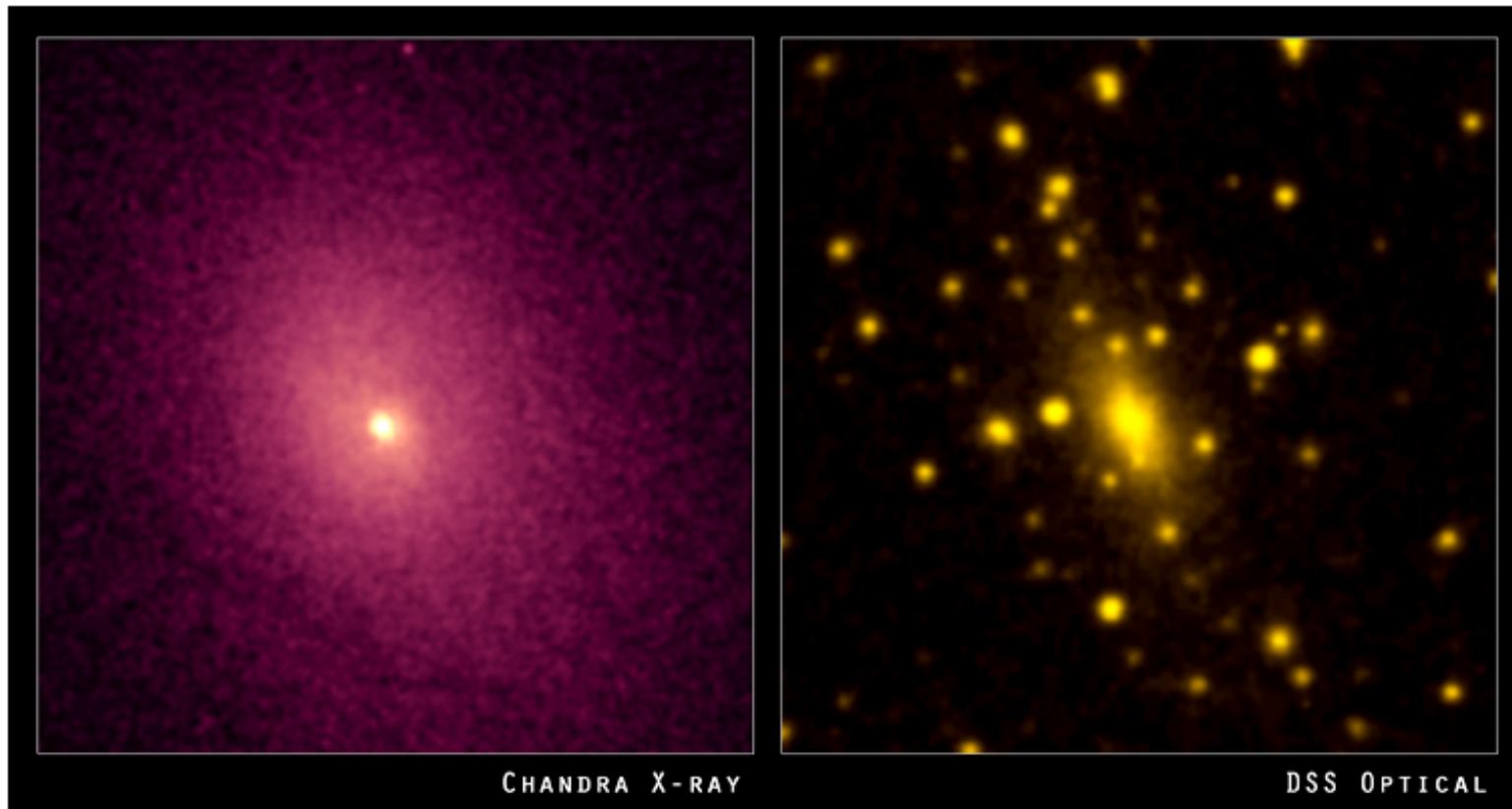
Spatial resolution: 6"

Energy Range 0.2 to 12 keV

High Spectral resolution at LowE $E/\Delta E = 300$

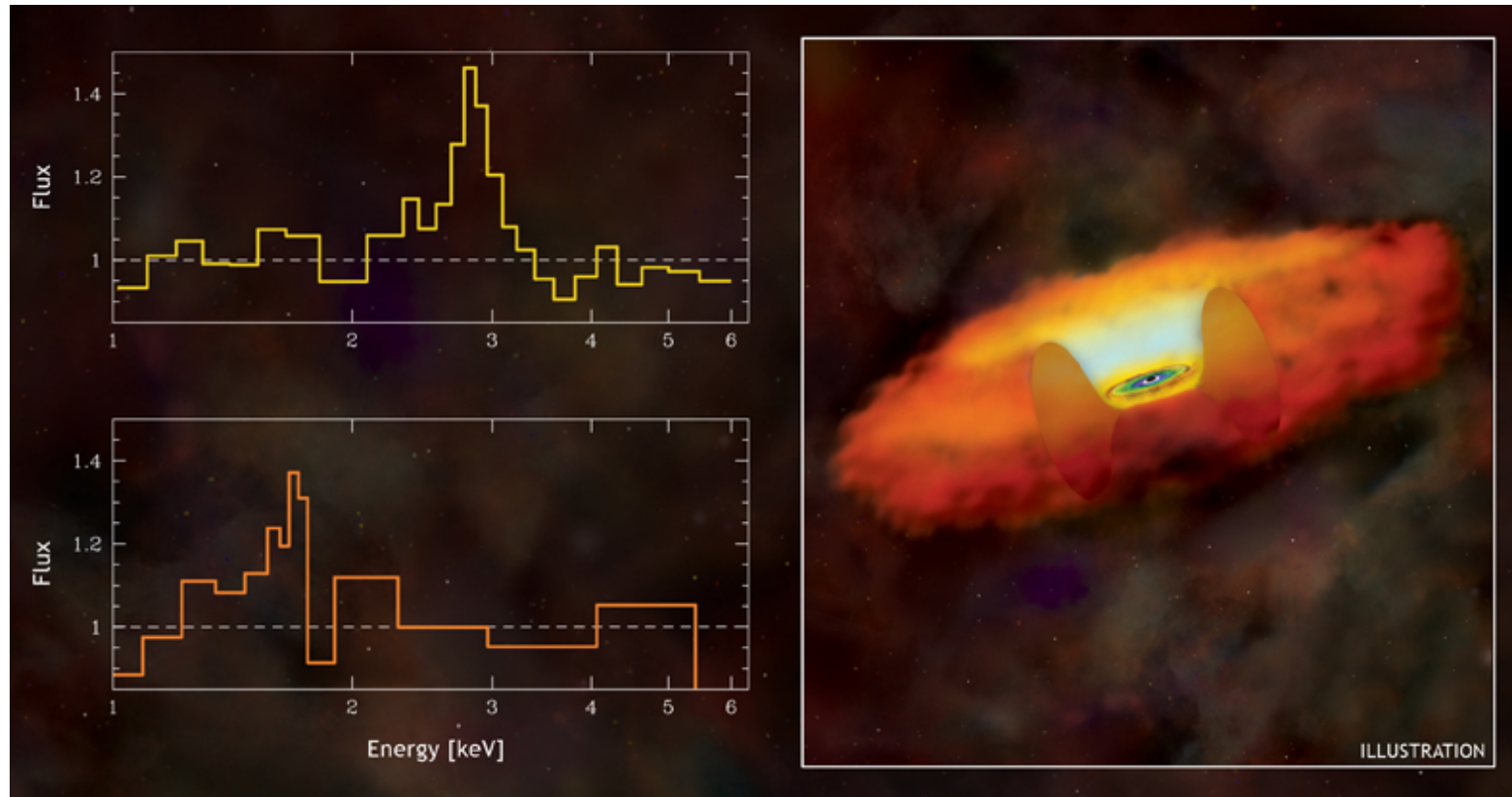
Wide FoV

Chandra results



The galaxy cluster Abell 2029 is composed of thousands of galaxies (optical image) enveloped in a gigantic cloud of hot gas (X-ray image)

Chandra results



The left side of the above graphic shows portions of X-ray spectra from a subset of 50 black holes about 9 billion light years away (upper panel), and another group of 22 black holes that are about 11 billion light years away (lower panel).

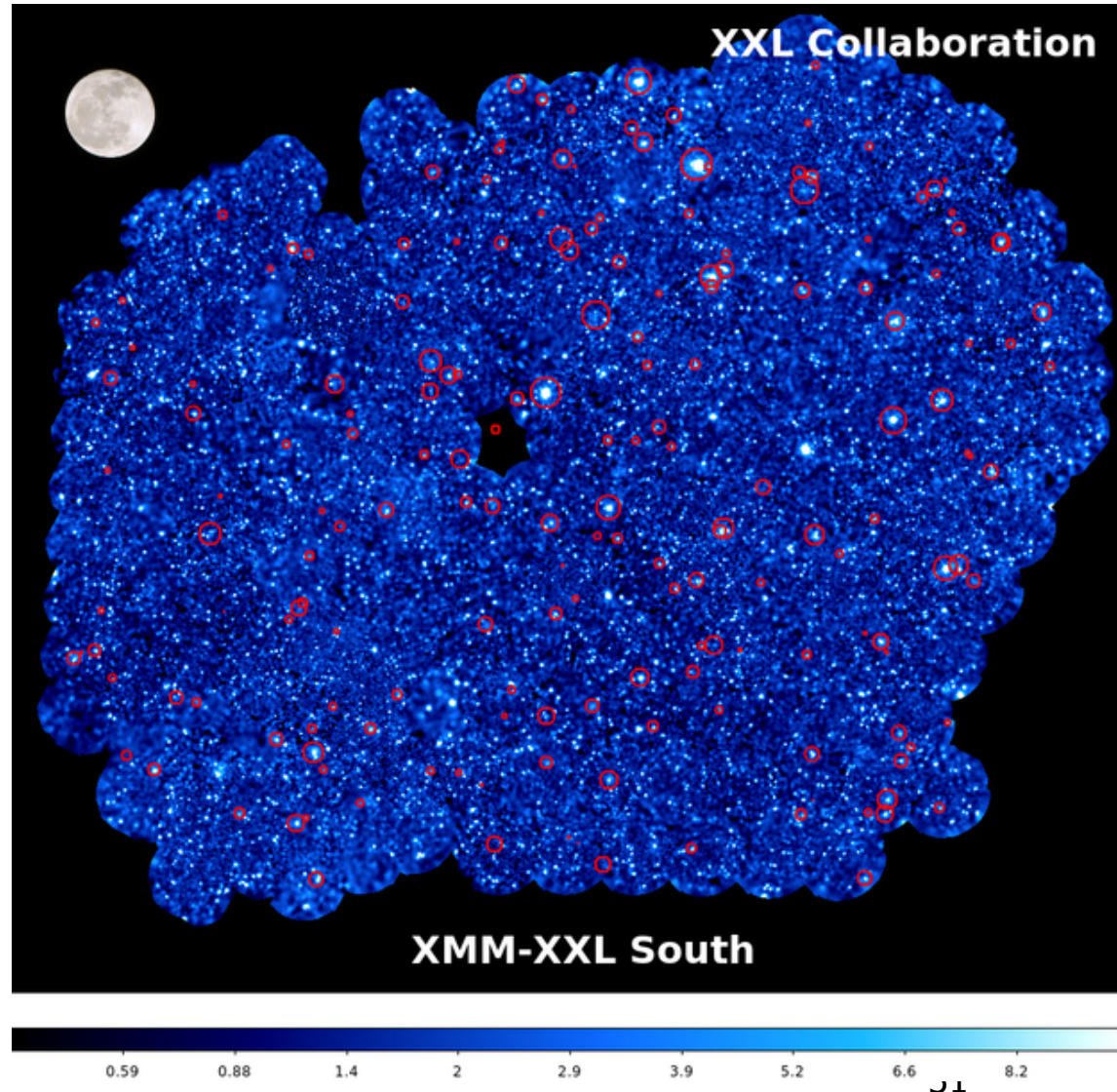
Chandra results



The Tycho and G292.0+1.8 supernova remnants show expanding debris from an exploded star and the associated shock waves. The images of the Crab Nebula and 3C58 show how neutron stars produced by a supernova can create clouds of high-energy particles.

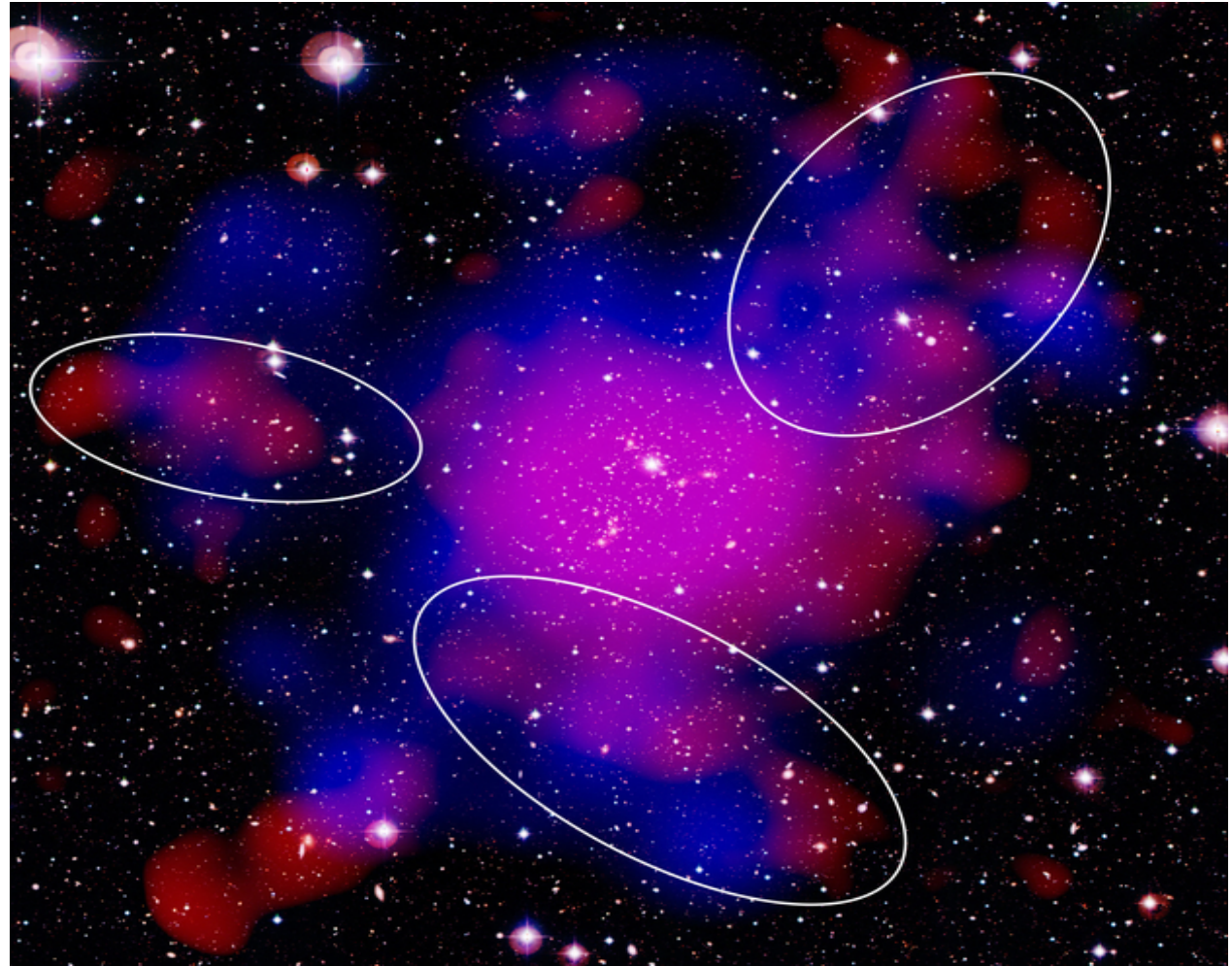
XMM results

- The XXL project, the largest XMM-Newton observing programme to date, set itself the ambitious task of mapping galaxy clusters back to a time when the Universe was just half of its present age. Its aim was to trace the evolution of the large-scale structure of the Universe.



XMM results

Components of the galaxy cluster Abell 2744, also known as the Pandora Cluster: galaxies (white), hot gas (red) and dark matter (blue).



X-ray science highlights

Chandra Images by Category



[Solar System](#) (9 listings)
Comets and planets



[Normal Stars & Star Clusters](#) (30 listings)
Stellar coronas, clusters of stars and hot gas produced by outflow from young stars.



[White Dwarfs & Planetary Nebulas](#) (10 listings)
Hot gas associated with the final stages of evolution of Sun-like stars, novae, and other white dwarfs in binary star systems.



[Supernovas & Supernova Remnants](#) (34 listings)
X-ray sources produced by the violent explosions of massive stars.



[Neutron Stars/X-ray Binaries](#) (26 listings)
Hot, isolated neutron stars, rotation-powered pulsars, and neutron stars accreting matter from a nearby companion star.



[Black Holes](#) (27 listings)
Stellar black holes, mid-mass black holes, and supermassive black holes.



[Milky Way Galaxy](#) (14 listings)
Images related to the Galactic Center and other features of the structure and evolution of the Milky Way Galaxy.



[Normal Galaxies & Starburst Galaxies](#) (39 listings)
Images of spiral, elliptical, and irregular galaxies that show X-ray sources associated with collapsed stars and star formation.



[Quasars & Active Galaxies](#) (33 listings)
Galaxies with unusually energetic activity, including high-energy jets, that is related to a central supermassive black hole.



[Groups & Clusters of Galaxies](#) (33 listings)
Vast clouds of hot gas embedded with numerous galaxies.

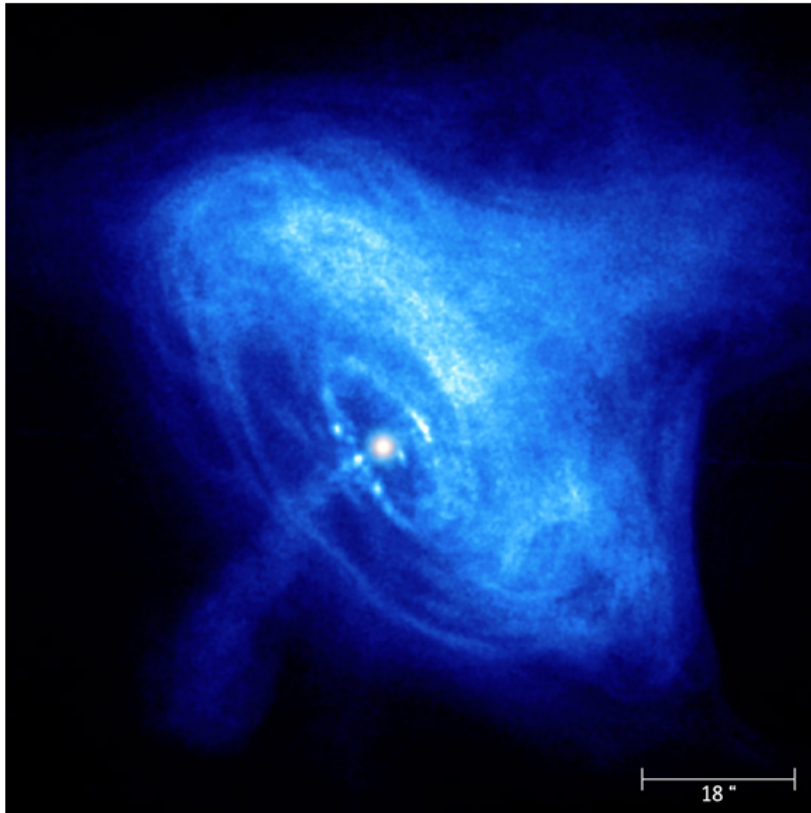


[Cosmology/Deep Fields/X-ray Background](#) (13 listings)
The sky as observed in X-rays is not dark, but gives off a glow thought to be from many distant sources. Deep surveys with the Chandra X-ray Observatory should reveal the cause of this glow.



[Miscellaneous](#) (8 listings)
Objects that don't fit in the above categories, such as brown dwarfs & gamma-ray bursts.

X-ray science highlights



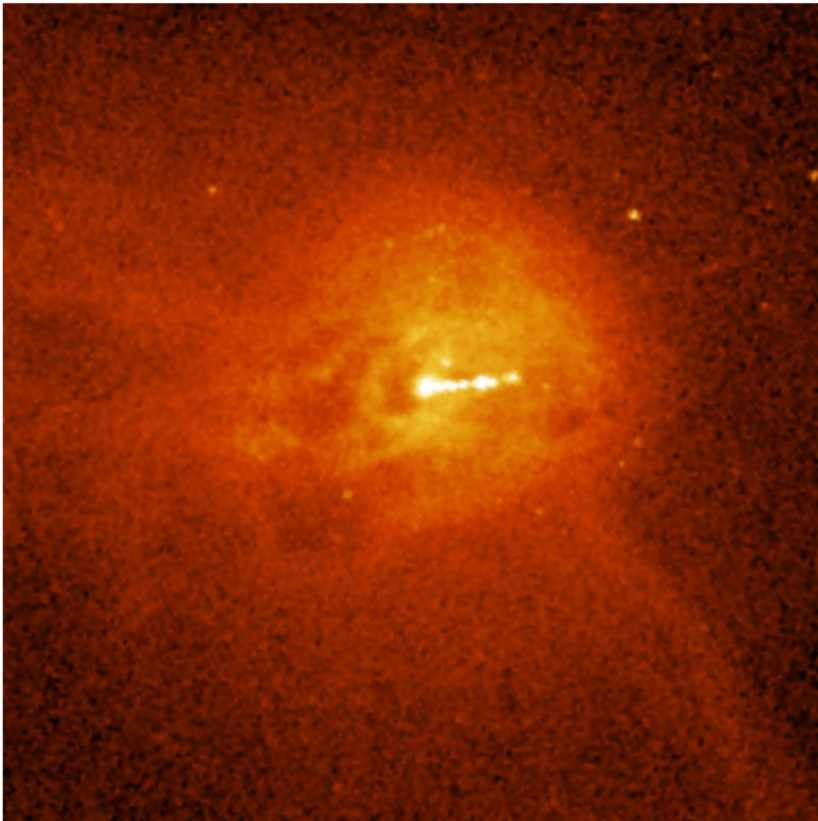
This image provides a view of the activity in the inner region around the Crab Nebula pulsar, a rapidly rotating neutron star seen as a bright white dot near the center of the images.

A wisp can be seen moving outward at half the speed of light from the upper right of the inner ring around the pulsar. The wisp appears to merge with a larger outer ring that is visible in both X-ray and optical images.

- The inner X-ray ring consists of about two dozen knots that form, brighten and fade. As a high-speed wind of matter and antimatter particles from the pulsar plows into the surrounding nebula, it creates a shock wave and forms the inner ring. Energetic shocked particles move outward to brighten the outer ring and produce an extended X-ray glow.

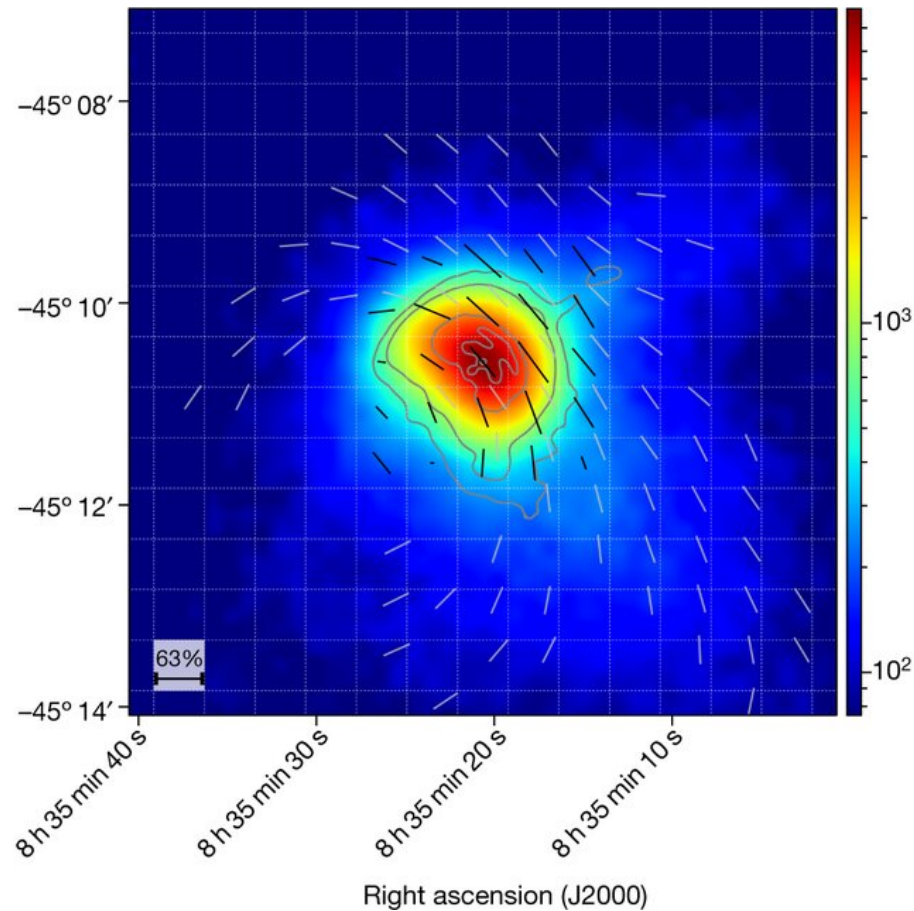
-

X-ray science highlights



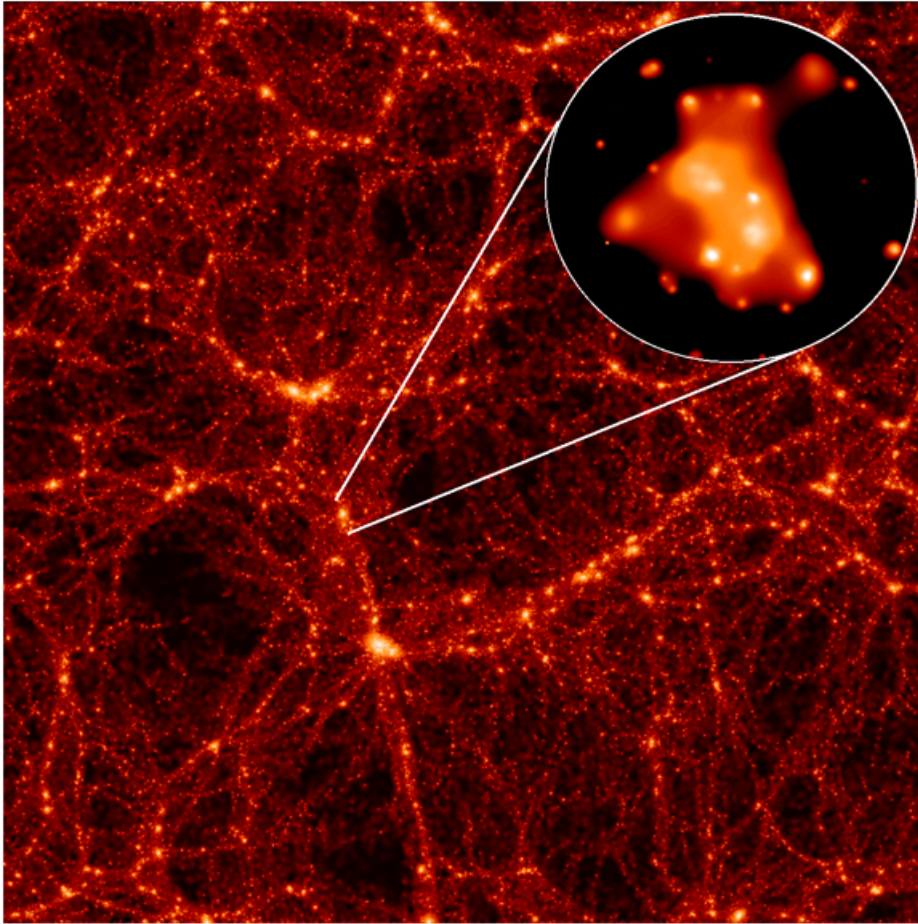
This close-up of M87 shows the region surrounding the jet of high-energy particles in more detail. The jet is thought to be pointed at a small angle to the line of sight, out of the plane of the image. This jet may be only the latest in a series of jets that have been produced as magnetized gas spirals in a disk toward the supermassive black hole

X-ray science highlights



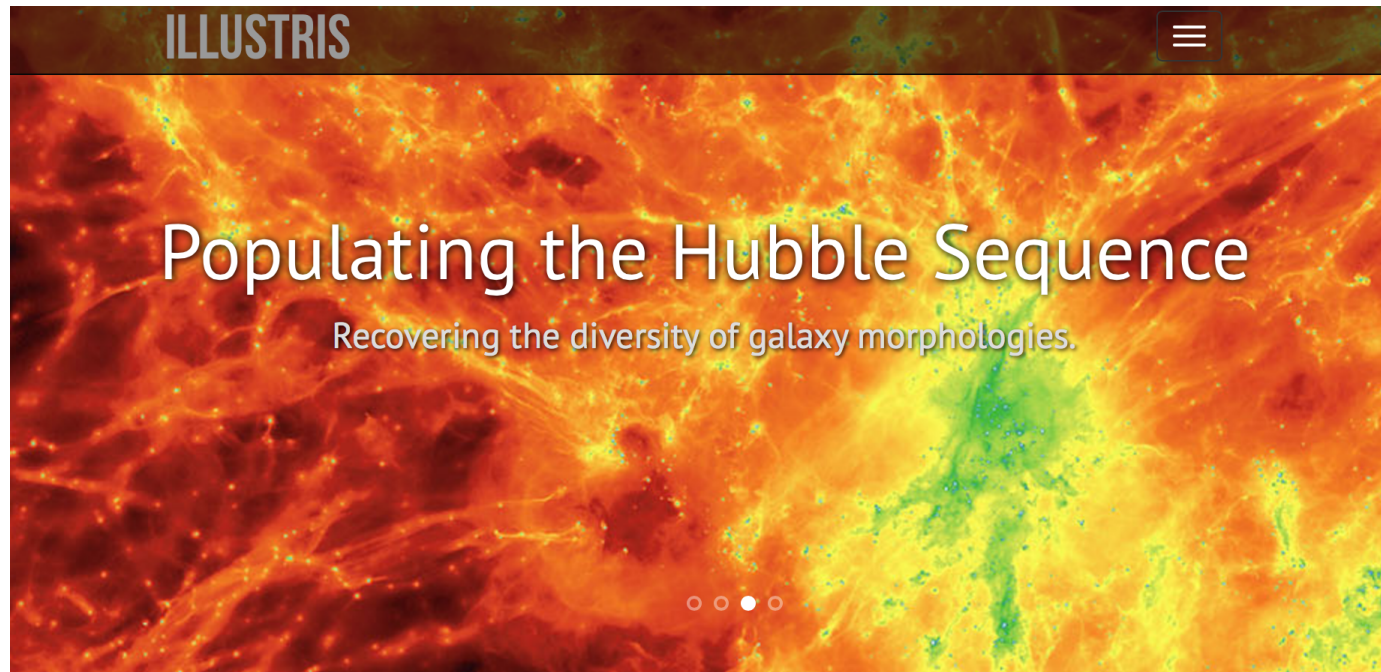
An image from NASA's Imaging X-ray Polarimetry Explorer (IXPE) observations of the Vela pulsar wind nebula. The colors represent different X-ray intensities, with the brightest regions in red and the faintest regions in blue. The black lines give the directions of the magnetic field based on the IXPE data and the silver lines give the directions of the magnetic field based on radio data from the Australia Telescope Compact Array. The grey contours show the X-ray intensities from Chandra data. The pulsar is located near the center of the brightest X-ray emission. Credit: Xie et al, 2022 (Nature)

X-ray science highlights



This image shows a computer simulation of a large volume of the Universe. An XMM-Newton X-ray image of a real galaxy cluster from the study is superimposed to illustrate the formation of galaxy clusters in the densest parts of the universe.

Dark Matter and Cosmo Simulations



Welcome

The Illustris project is a large cosmological simulation of galaxy formation, completed in late 2013, using a state of the art numerical code and a comprehensive physical model. Building on several years of effort by members of the collaboration, the Illustris simulation represents an unprecedented combination of high resolution, total volume, and physical fidelity. The [About](#) page contains detailed descriptions of the project, for both the general public and researchers in the field.

On this website we present the scientific motivation behind the project, a list of the collaboration members, key results and references, movies and images created from the simulation data, information on upcoming public data access, and tools for interactive data exploration. The short video below is a compilation made from some of the movies available on the [Media](#) page.

<http://www.illustris-project.org>

<http://www.tng-project.org>

Dark Matter and Cosmo Simulations

Numerical Simulations of the Dark Universe: State of the Art and the Next Decade

Michael Kuhlen^a, Mark Vogelsberger^b, Raul Angulo^{c,d}

^a*Theoretical Astrophysics Center, University of California Berkeley, Hearst Field Annex, Berkeley, CA 94720, USA*

^b*Hubble Fellow, Harvard-Smithsonian Center for Astrophysics, 60 Garden Street, Cambridge, MA 02138, USA*

^c*Max-Planck-Institute for Astrophysics, Karl-Schwarzschild-Str. 1, 85740 Garching, Germany*

^d*Kavli Institute for Particle Astrophysics and Cosmology, Stanford University, Menlo Park, CA 94025, USA*

Abstract

We present a review of the current state of the art of cosmological dark matter simulations, with particular emphasis on the implications for dark matter detection efforts and studies of dark energy. This review is intended both for particle physicists, who may find the cosmological simulation literature opaque or confusing, and for astro-physicists, who may not be familiar with the role of simulations for observational and experimental probes of dark matter and dark energy. Our work is complementary to the contribution by M. Baldi in this issue, which focuses on the treatment of dark energy and cosmic acceleration in dedicated N-body simulations.

Truly massive dark matter-only simulations are being conducted on national supercomputing centers, employing from several billion to over half a trillion particles to simulate the formation and evolution of cosmologically representative volumes (cosmic scale) or to zoom in on individual halos (cluster and galactic scale). These simulations cost millions of core-hours, require tens to hundreds of terabytes of memory, and use up to petabytes of disk storage. Predictions from such simulations touch on almost every aspect of dark matter and dark energy studies, and we give a comprehensive overview of this connection. We also discuss the limitations of the cold and collisionless DM-only approach, and describe in some detail efforts to include different particle physics as well as baryonic physics in cosmological galaxy formation simulations, including a discussion of recent results highlighting how the distribution of dark matter in halos may be altered. We end with an outlook for the next decade, presenting our view of how the field can be expected to progress.

Suzaku

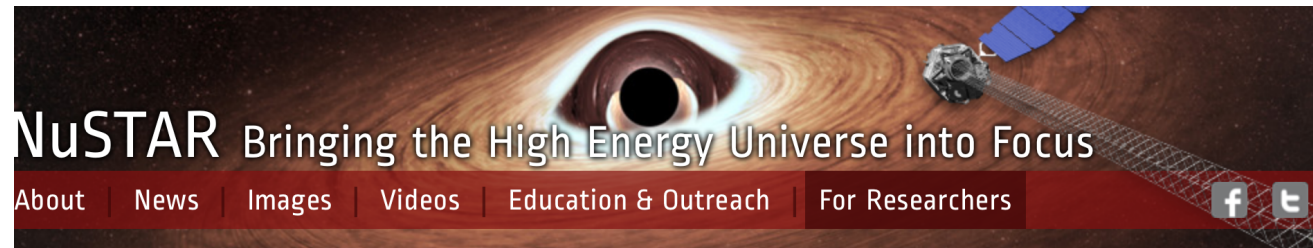
- Suzaku launched on July 10, 2005. Before launch it was called Astro-E2, and the name was changed to Suzaku shortly after the successful launch.
- Suzaku's four CCD cameras for low-energy X-rays and detector for high-energy X-rays continue to study the X-ray sky. In scientists' words, Suzaku is designed for "broad-band, high-sensitivity, high-resolution" spectroscopy.



<http://www.isas.jaxa.jp/e/enterp/missions/suzaku/>

NuSTAR

- The NuSTAR (Nuclear Spectroscopic Telescope Array) mission has deployed the first orbiting telescopes to focus light in the high energy X-ray (3 - 79 keV) region of the electromagnetic spectrum. Our view of the universe in this spectral window has been limited because previous orbiting telescopes have not employed true focusing optics, but rather have used coded apertures that have intrinsically high backgrounds and limited sensitivity.



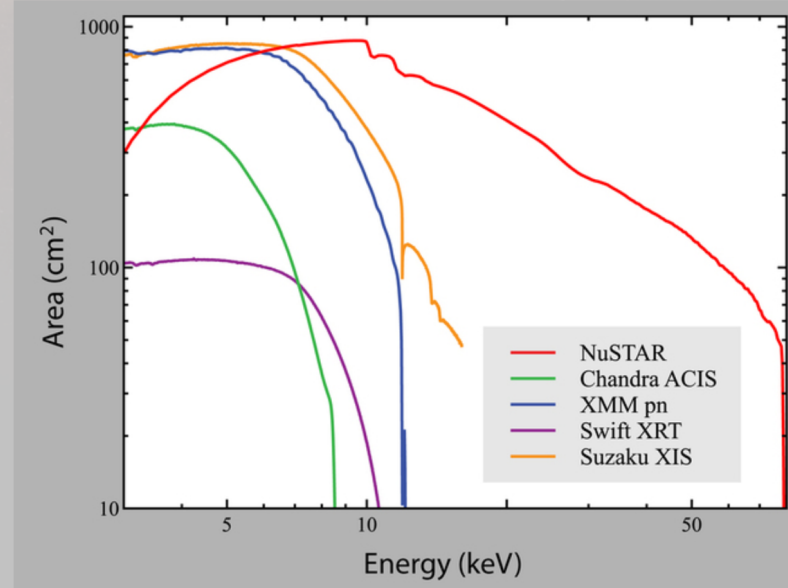
NuSTAR Bringing the High Energy Universe into Focus

About | News | Images | Videos | Education & Outreach | For Researchers

Science Operations Center
NuSTAR at the HEASARC
Targets of Opportunity
For Proposers
Legacy Surveys
Publications
Technical Publications

Researchers

The primary reference for NuSTAR is [Harrison, F.A. et al. \(2013; ApJ, 770, 103\)](#).



Area (cm²) vs Energy (keV) plot showing the performance of NuSTAR and other X-ray telescopes. The plot shows Area (cm²) on a logarithmic y-axis (10 to 1000) versus Energy (keV) on a logarithmic x-axis (1 to 100). The legend indicates:

- NuSTAR (Red line)
- Chandra ACIS (Green line)
- XMM pn (Blue line)
- Swift XRT (Purple line)
- Suzaku XIS (Orange line)

Energy (keV)	NuSTAR Area (cm ²)	Chandra ACIS Area (cm ²)	XMM pn Area (cm ²)	Swift XRT Area (cm ²)	Suzaku XIS Area (cm ²)
1	~300	~300	~300	~100	~300
5	~600	~300	~600	~100	~600
10	~800	~30	~100	~10	~100
50	~100	~0	~0	~0	~0
79	~10	~0	~0	~0	~0

<http://www.nustar.caltech.edu/>

MAXI

The Monitor of All-sky X-ray Image, MAXI, is the first experiment installed on the Japanese Experiment Module Exposed Facility (JEM-EF or Kibo-EF) on the International Space Station (ISS) and the first high energy astrophysical experiment placed on the space station.

The main objectives of MAXI are early detection of X-ray transient events, and monitoring the intensity fluctuation of known X-ray sources over long periods by scanning the all sky in soft and hard X-ray.

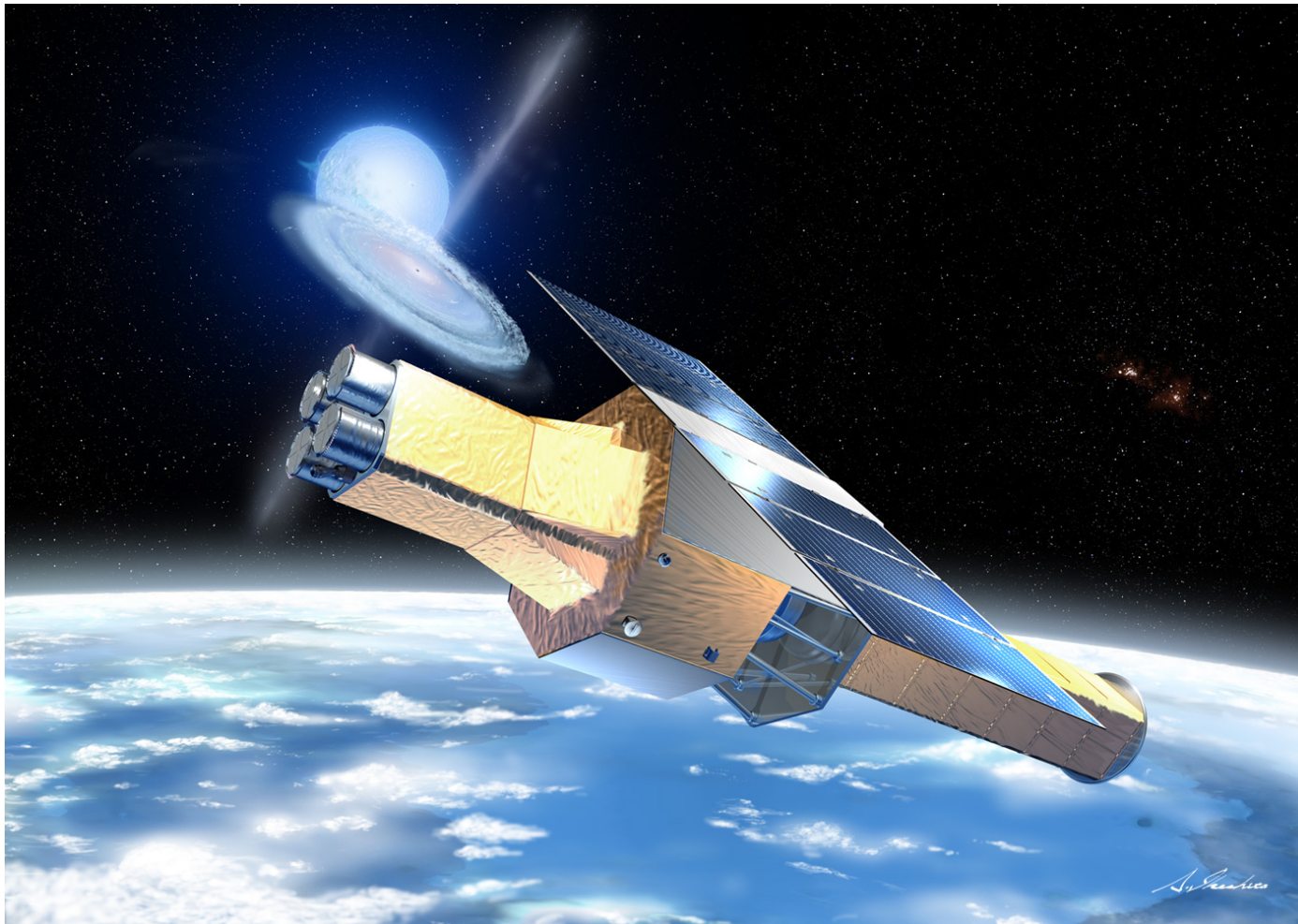
- two semi-circular arc-shaped X-ray slit cameras with wide FOVs. In the 92 minutes it takes the ISS to orbit the earth, MAXI gets a 360 deg image of the entire sky.
- two kinds of X-ray detectors, collecting events from the slit cameras: a gas proportional counters, the Gas Slit Camera (GSC; 2-30 keV), and a X-ray CCD, Solid-state Slit Camera (SSC; 0.5-12 keV).



S127E009561

<https://heasarc.gsfc.nasa.gov/docs/maxi/>

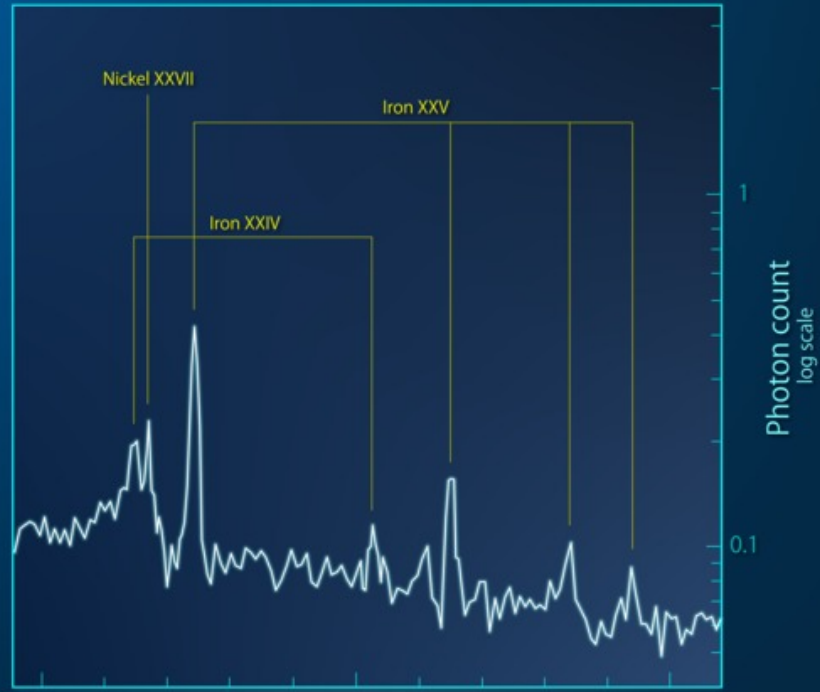
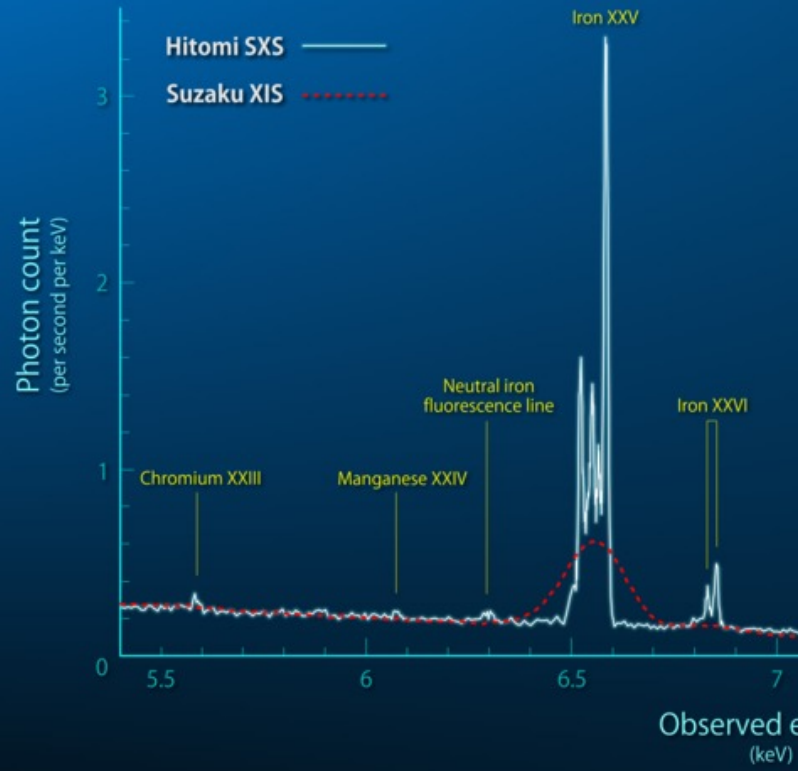
Astro-H – Hitomi



<http://astro-h.isas.jaxa.jp/en/>



Perseus Galaxy Cluster X-ray Spectra



<https://svs.gsfc.nasa.gov/12297>

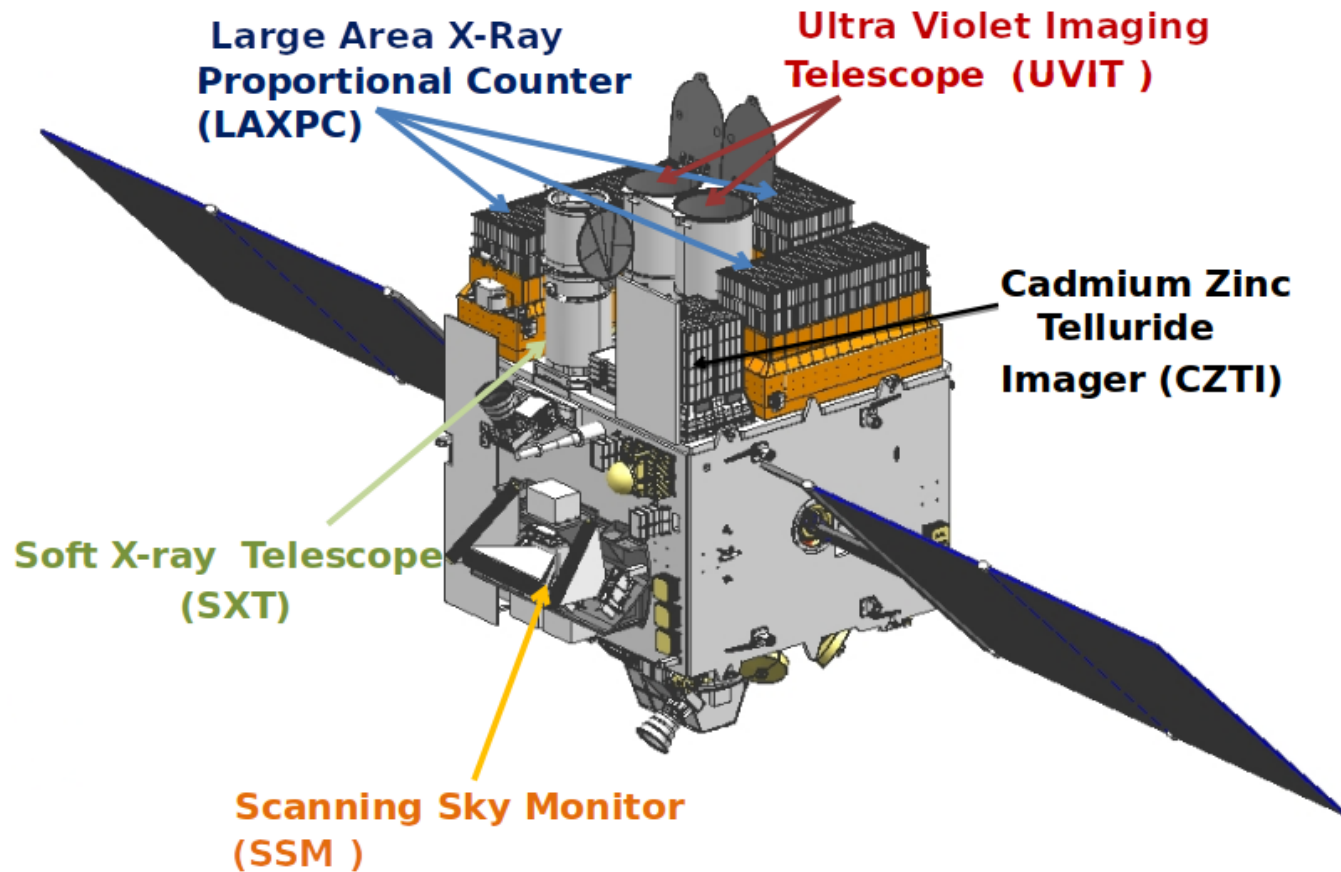
NICER



<https://heasarc.gsfc.nasa.gov/docs/nicer/>

ASTROSAT

<https://www.isro.gov.in/Spacecraft/astrosat>



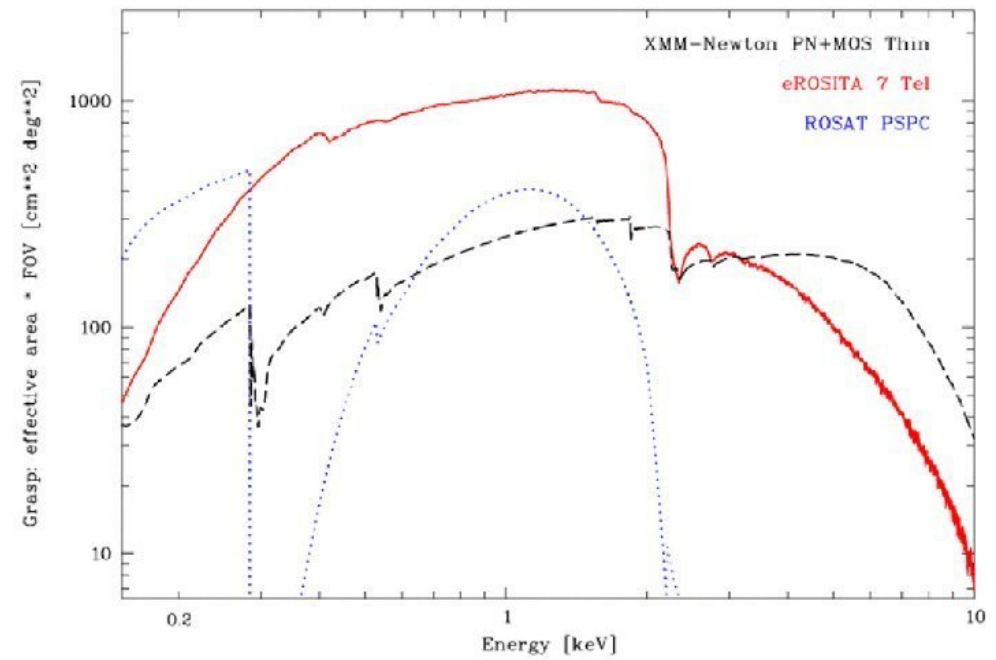
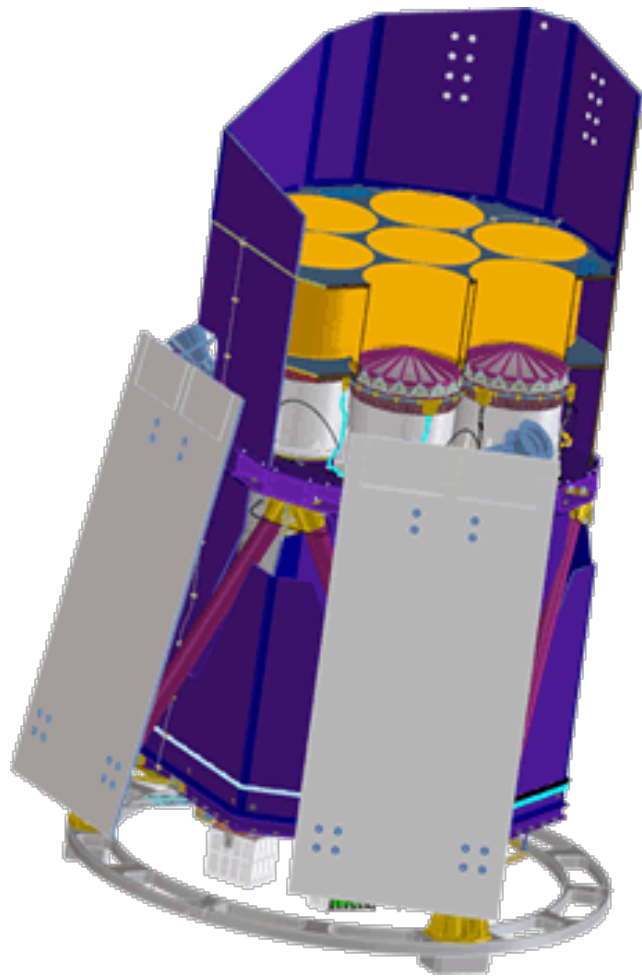
https://astrobrowse.issdc.gov.in/astro_archive/archive/Home.jsp

HMXT



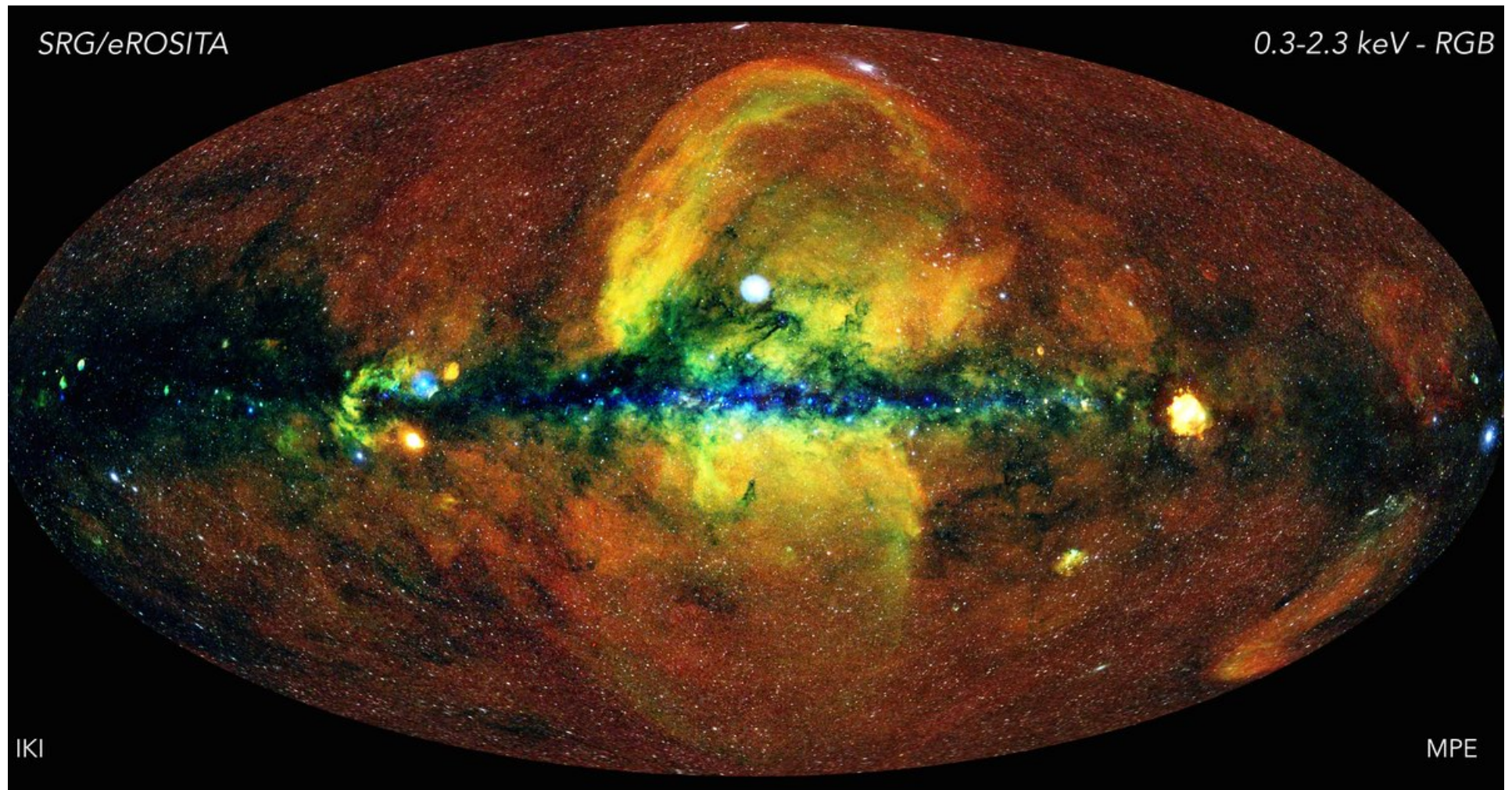
<http://hxmtcn.ihep.ac.cn/>

eROSITA



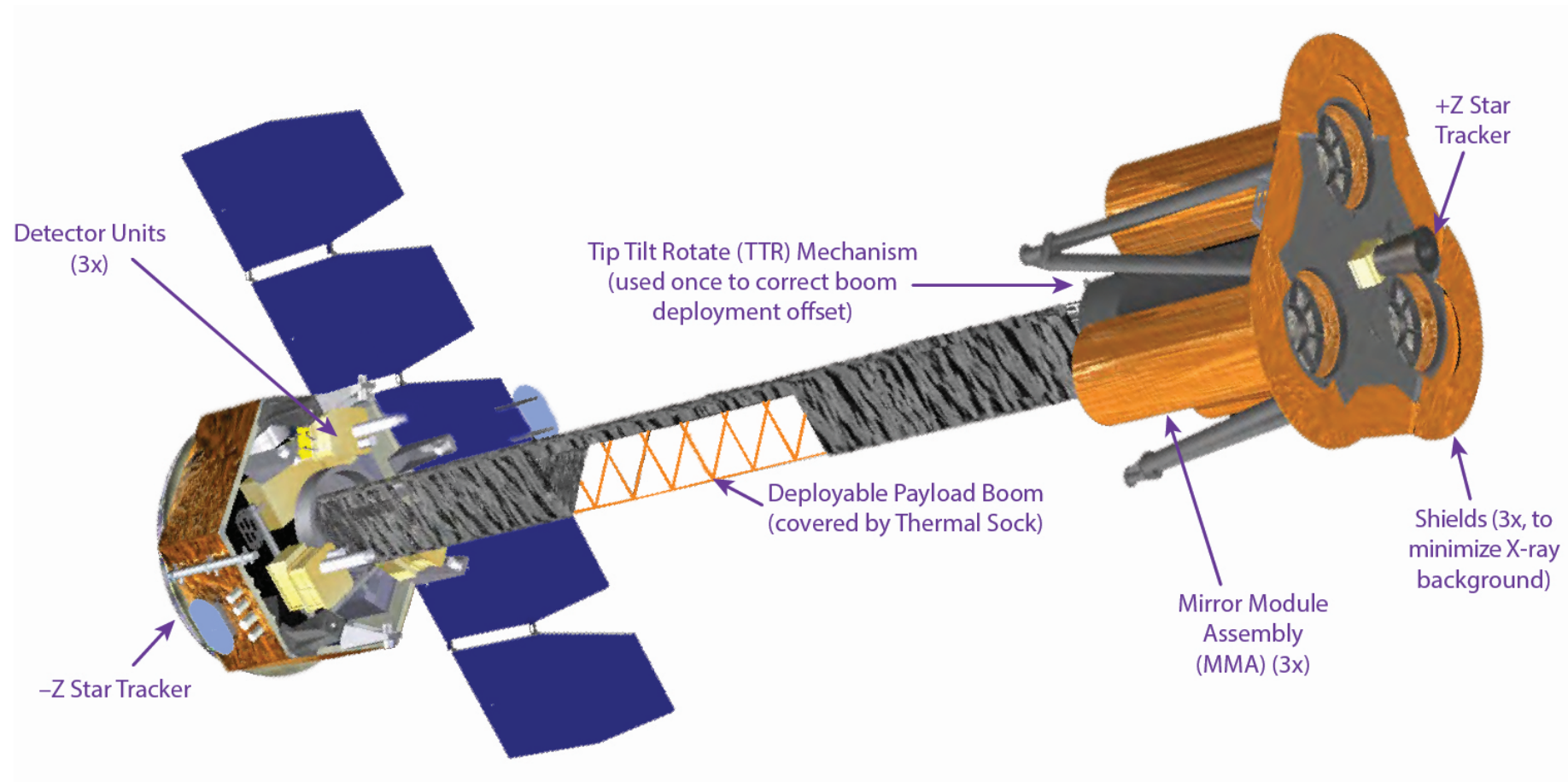
<https://www.mpe.mpg.de/eROSITA>

eROSITA survey



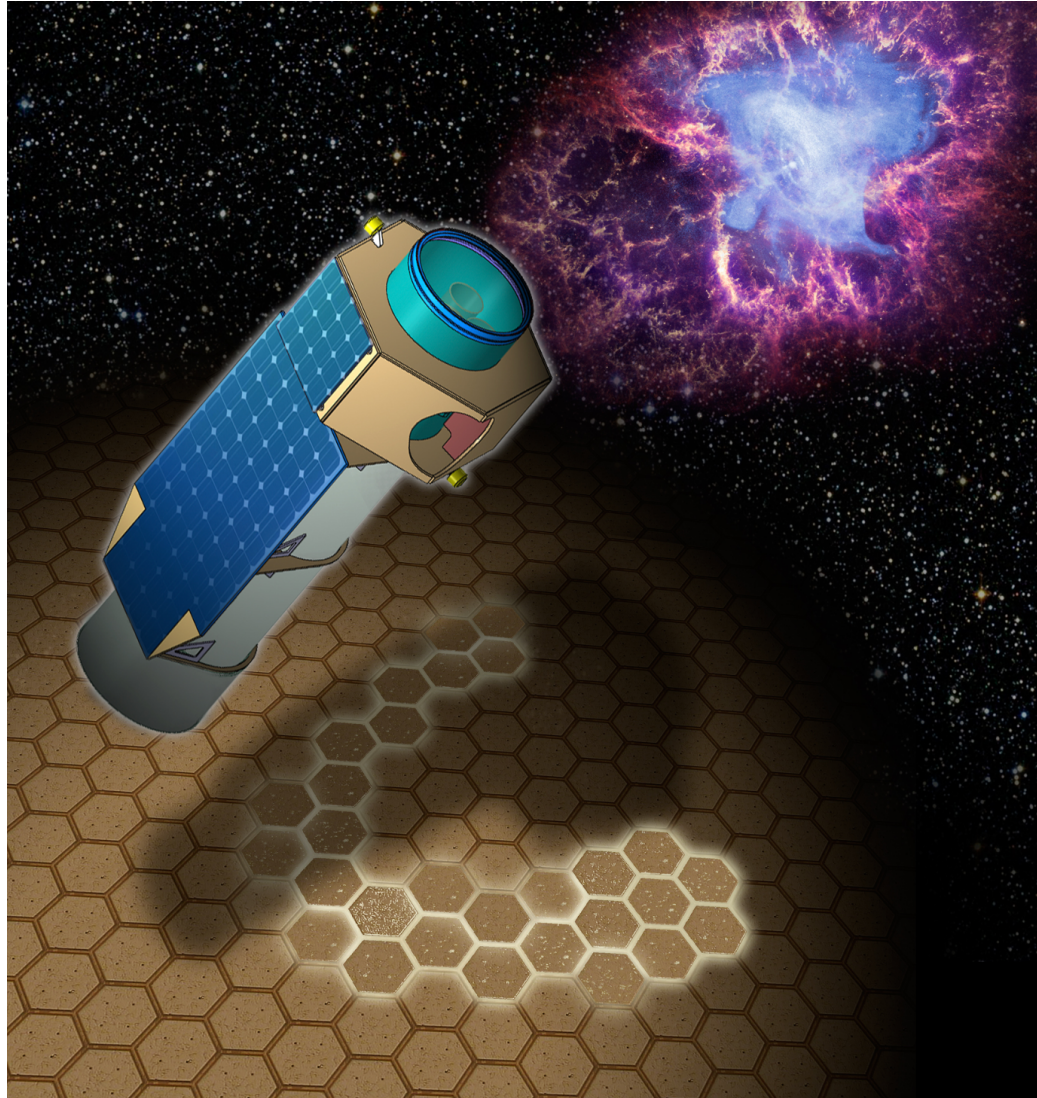
<https://www.mpe.mpg.de/7461761/news20200619>

IXPE



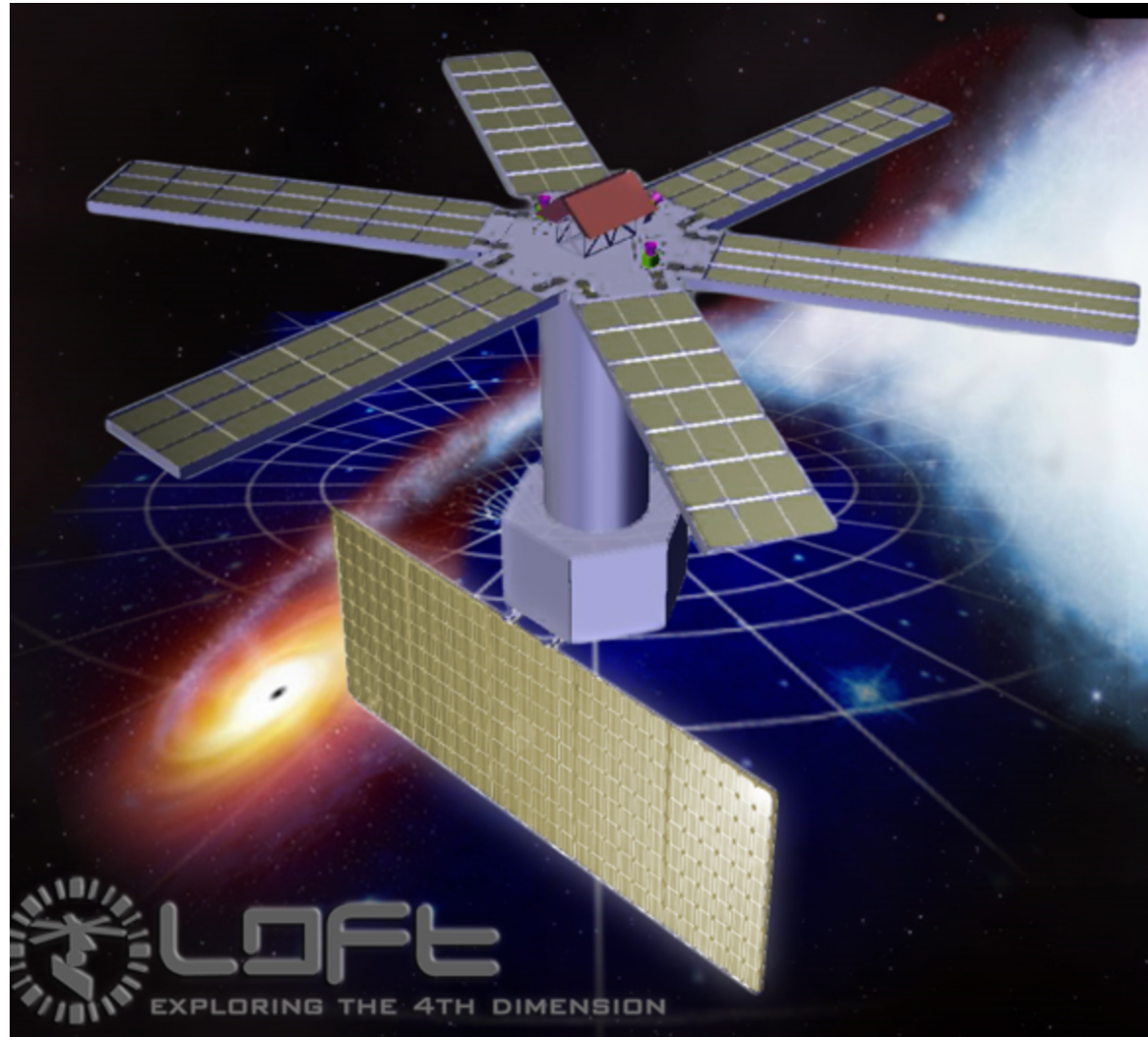
<https://wwwastro.msfc.nasa.gov/ixpe/>

XIPE



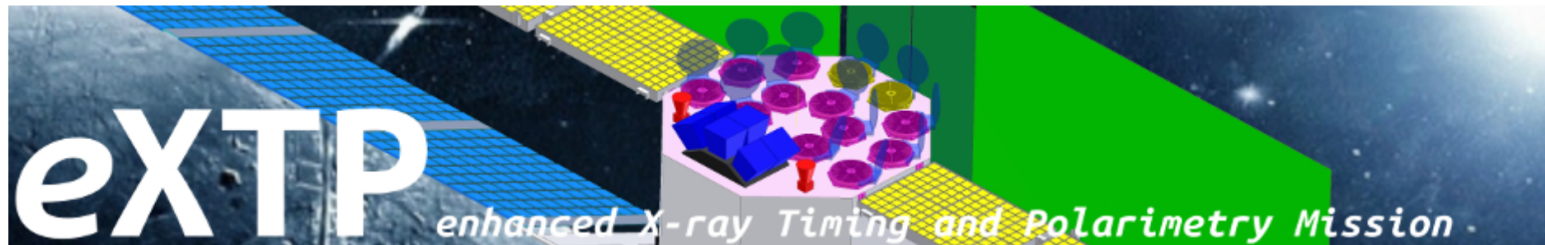
<http://www.isdc.unige.ch/xipe/>

LOFT



<http://www.isdc.unige.ch/loft/>

eXTP



The eXTP Mission

[The eXTP mission](#)
[The eXTP Payload](#)
[Science with eXTP](#)
[SPIE 2016 paper](#)
[Publications on eXTP](#)
[Public Response Files](#)

eXTP Teams

[WG1 - Dense Matter](#)
[WG2 - Strong Field Gravity](#)
[WG3 - Strong Magnetism](#)
[WG4 - Observatory Science](#)
[WG5 - Synergy with GWs](#)
[WG6 - Simulations](#)
[Instrument Working Group Consortium](#)

The eXTP Mission

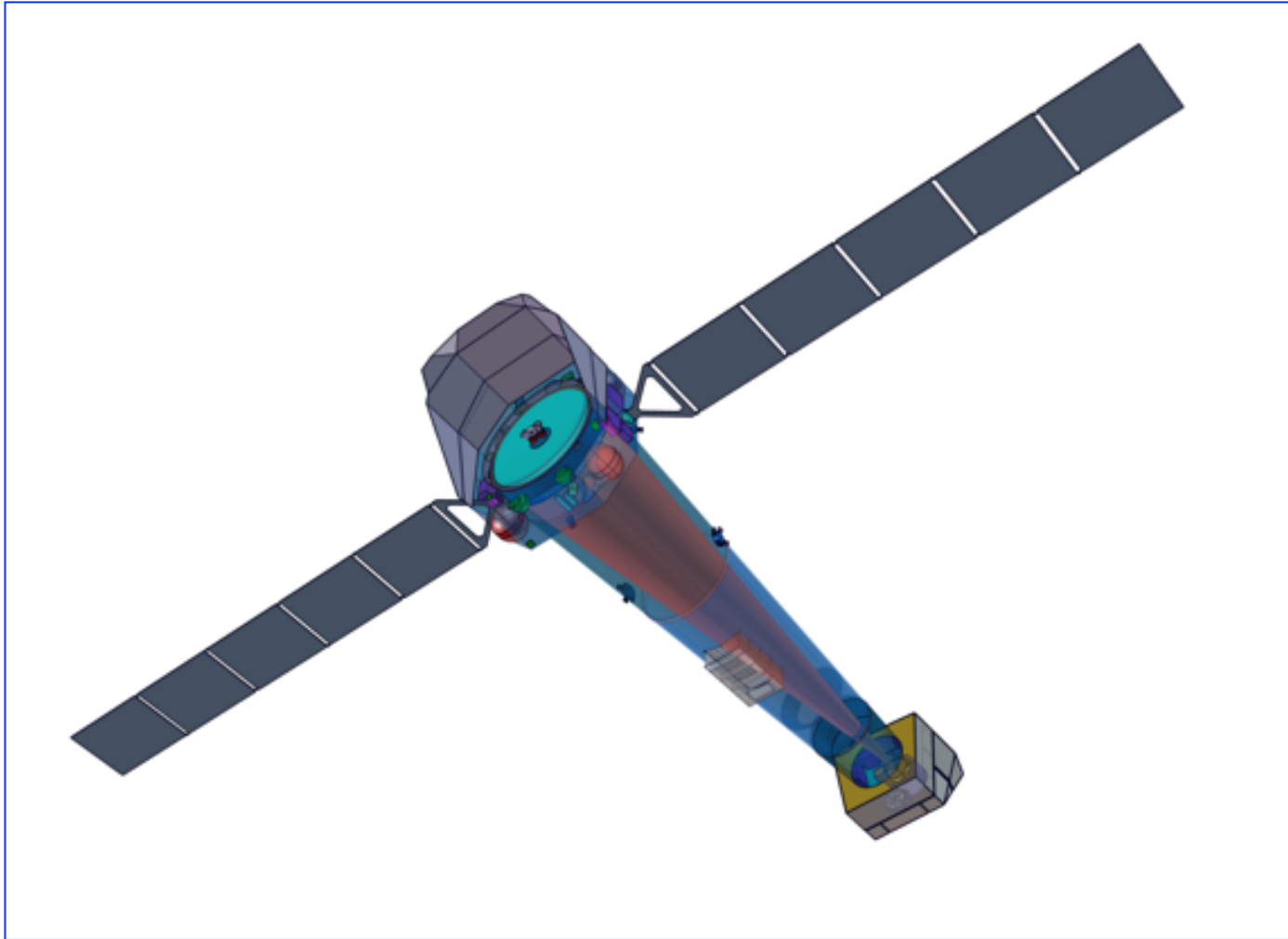
The [enhanced X-ray Timing and Polarimetry mission \(eXTP\)](#) is a science mission designed to study the state of matter under extreme conditions of density, gravity and magnetism. Primary goals are the determination of the equation of state of matter at supra-nuclear density, the measurement of QED effects in highly magnetized star, and the study of accretion in the strong-field regime of gravity. Primary targets include isolated and binary neutron stars, strong magnetic field systems like magnetars, and stellar-mass and supermassive black holes.

The mission carries a unique and unprecedented suite of state-of-the-art scientific instruments enabling for the first time ever the simultaneous spectral-timing-polarimetry studies of cosmic sources in the energy range from 0.5-30 keV (and beyond). Key elements of the payload are:

- **the Spectroscopic Focusing Array (SFA)**: a set of 11 X-ray optics operating in the 0.5-10 keV energy band with a field-of-view (FoV) of 12 arcmin each and a total effective area of $\sim 0.9 \text{ m}^2$ and 0.6 m^2 at 2 keV and 6 keV respectively. The telescopes are equipped with Silicon Drift Detectors offering $< 180 \text{ eV}$ spectral resolution.
- **the Large Area Detector (LAD)**: a deployable set of 640 Silicon Drift Detectors, achieving a total effective area of $\sim 3.4 \text{ m}^2$ between 6 and 10 keV. The operational energy range is 2-30 keV and the achievable spectral resolution better than 250 eV. This is a non-imaging instrument, with the FoV limited to $< 1^\circ$ FWHM by the usage of compact capillary plates.
- **the Polarimetry Focusing Array (PFA)**: a set of 2 X-ray telescope, achieving a total effective area of 250 cm^2 at 2 keV, equipped with imaging gas pixel photoelectric polarimeters. The FoV of each telescope is 12 arcmin and the operating energy range is 2-10 keV.
- **the Wide Field Monitor (WFM)**: a set of 3 coded mask wide field units, equipped with position-sensitive Silicon Drift Detectors, covering in total a FoV of 3.7 sr and operating in the energy range 2-50 keV.

<http://www.isdc.unige.ch/extp/>

Athena



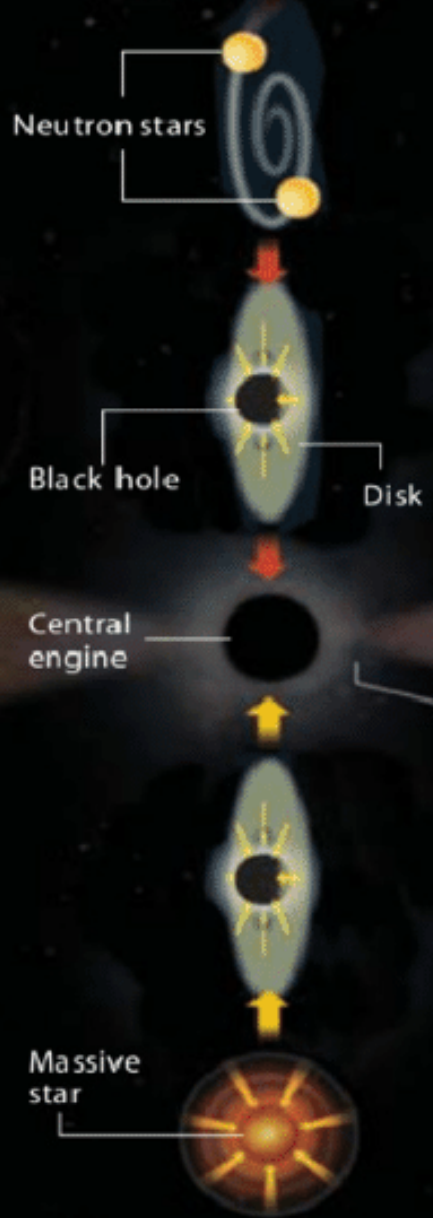
<https://www.the-athena-x-ray-observatory.eu>

XRISM

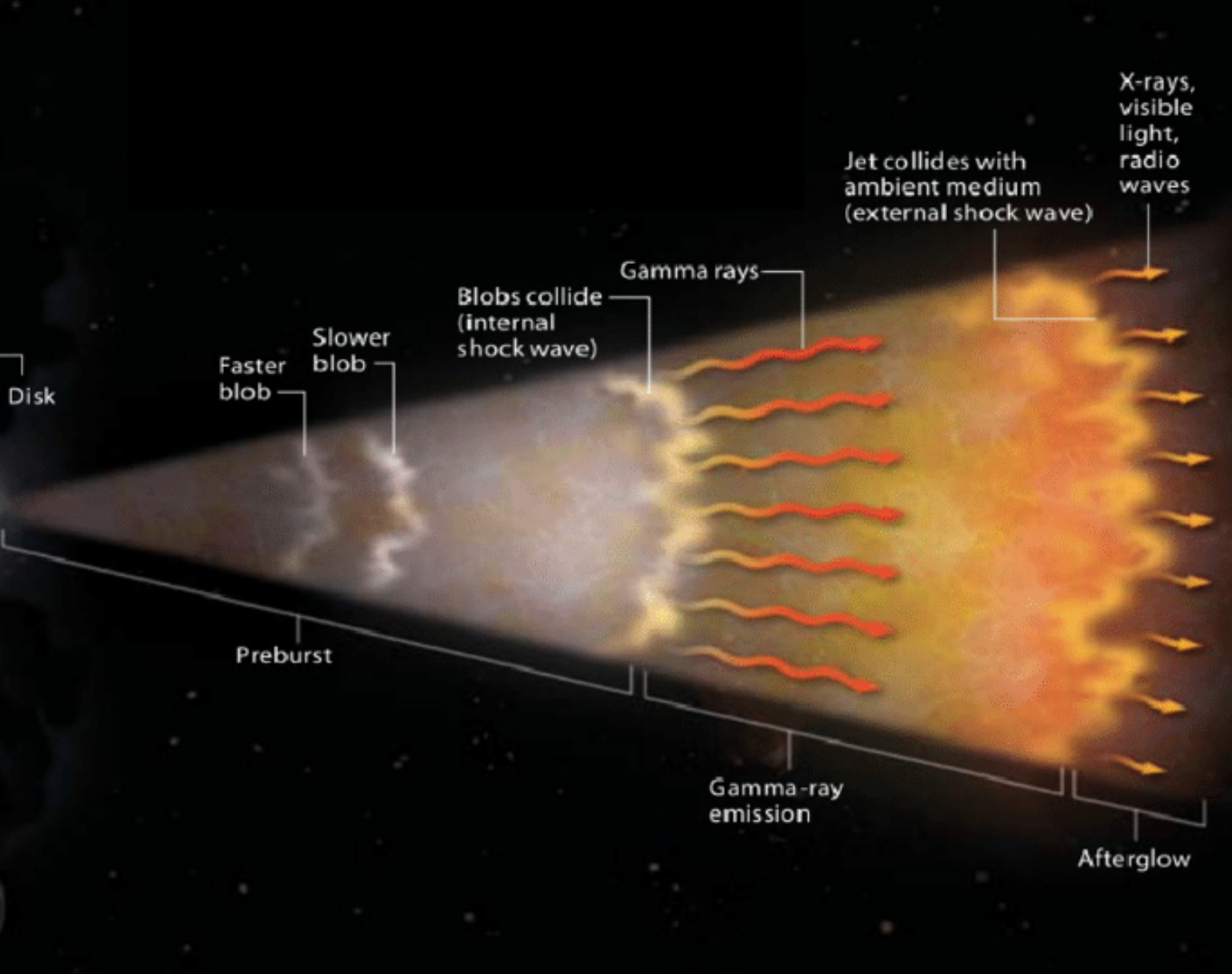
<https://heasarc.gsfc.nasa.gov/docs/xrism/>

Astrofisica Nucleare e Subnucleare
Neutrino Astrophysics

Merger scenario



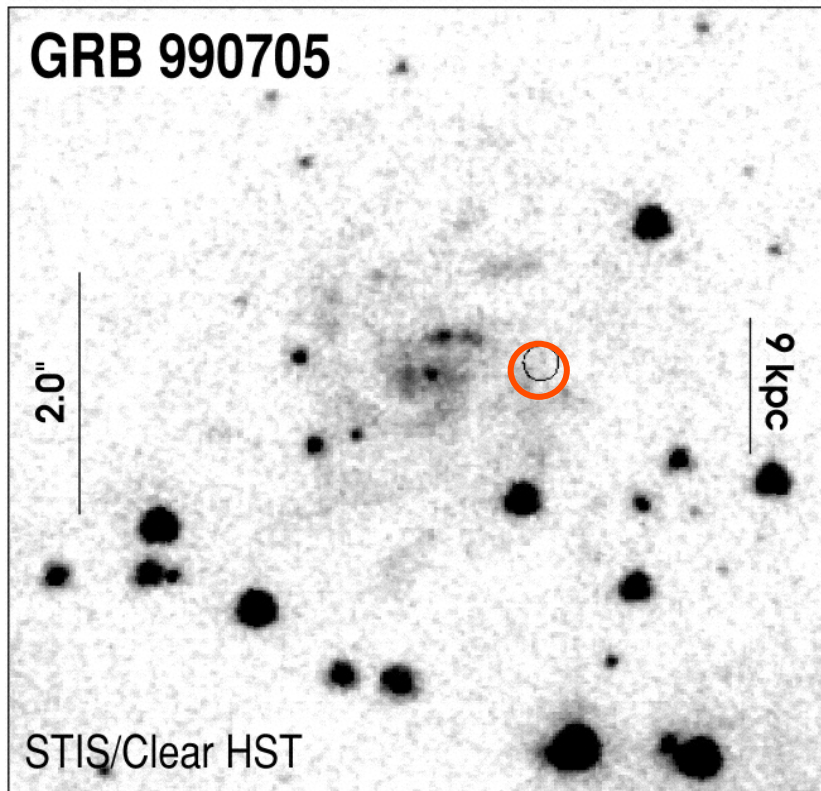
Hypernova scenario



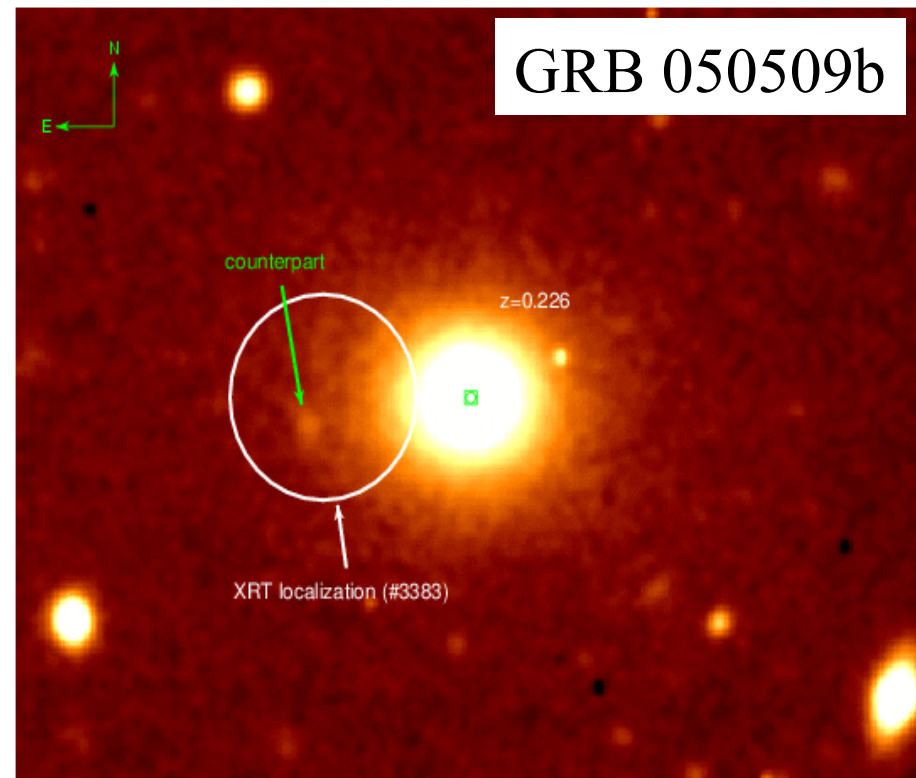
Unveiling the GRB progenitors

- host galaxies long GRBs: blue, usually regular and high star forming, GRB located in star forming regions
- host galaxies of short GRBs: elliptical, irregular galaxies, away from star forming region

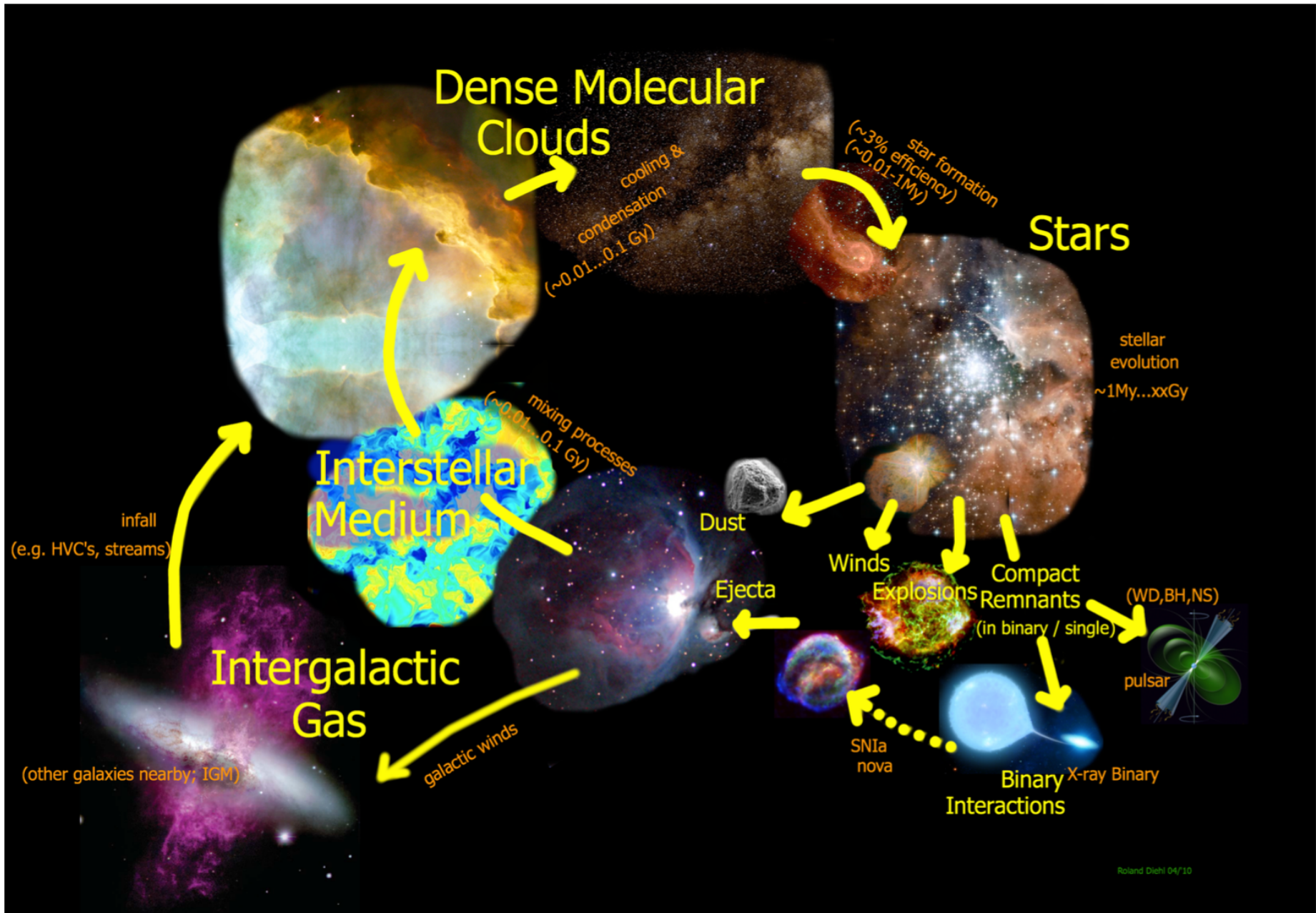
Long



Short



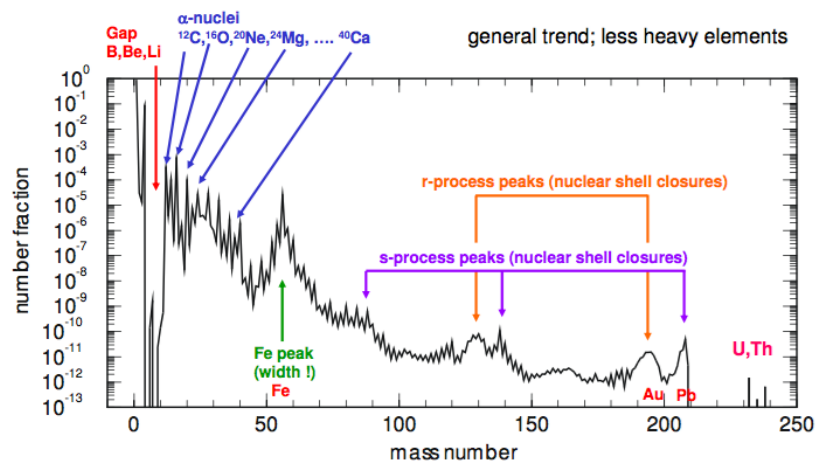
How Stars Shape Galaxies



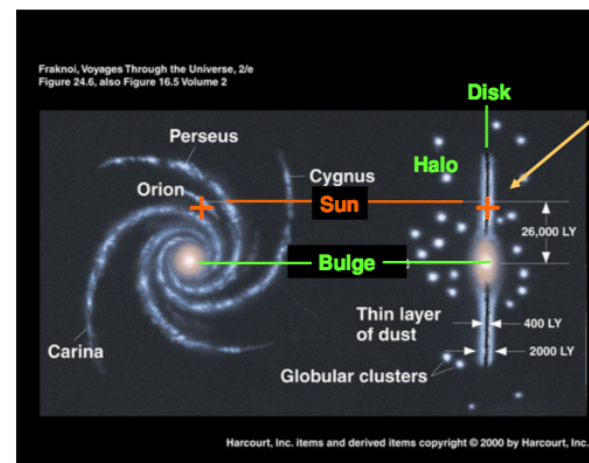
What is Nuclear Astrophysics?

- Nuclear astrophysics aims at understanding the nuclear processes that take place in the universe.
- These nuclear processes generate energy in stars and contribute to the nucleosynthesis of the elements and the evolution of the galaxy.

Hydrogen mass fraction	$X = 0.71$
Helium mass fraction	$Y = 0.28$
Metallicity (mass fraction of everything else)	$Z = 0.019$
Heavy Elements (beyond Nickel) mass fraction	$4E-6$



3. The solar abundance distribution

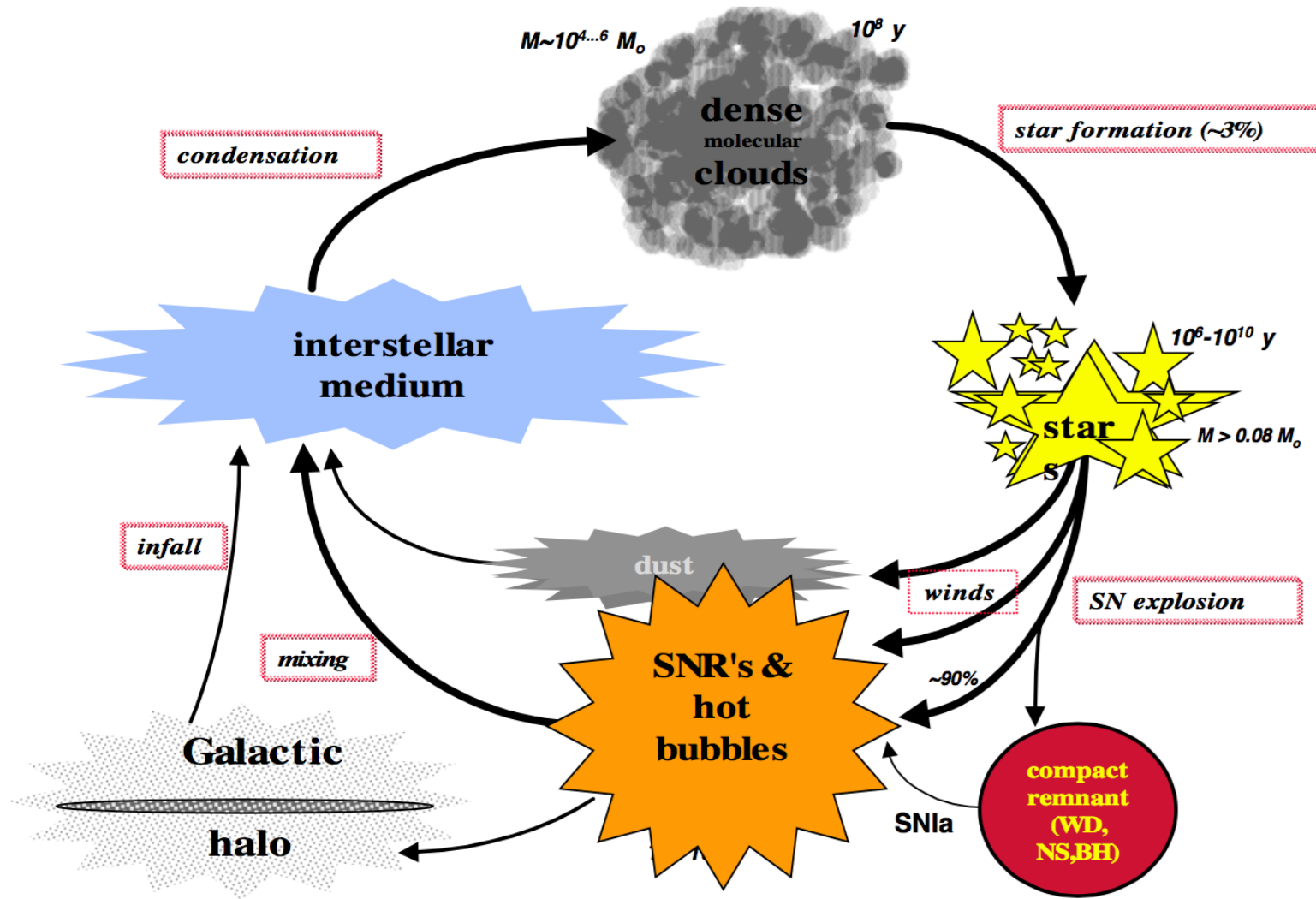


solar abundances:

Elemental (and isotopic) composition of Galaxy at location of solar system at the time of its formation

K. Lodders, *Astrophys. J.* **591**, 1220-1247 (2003)

Cosmic Cycle

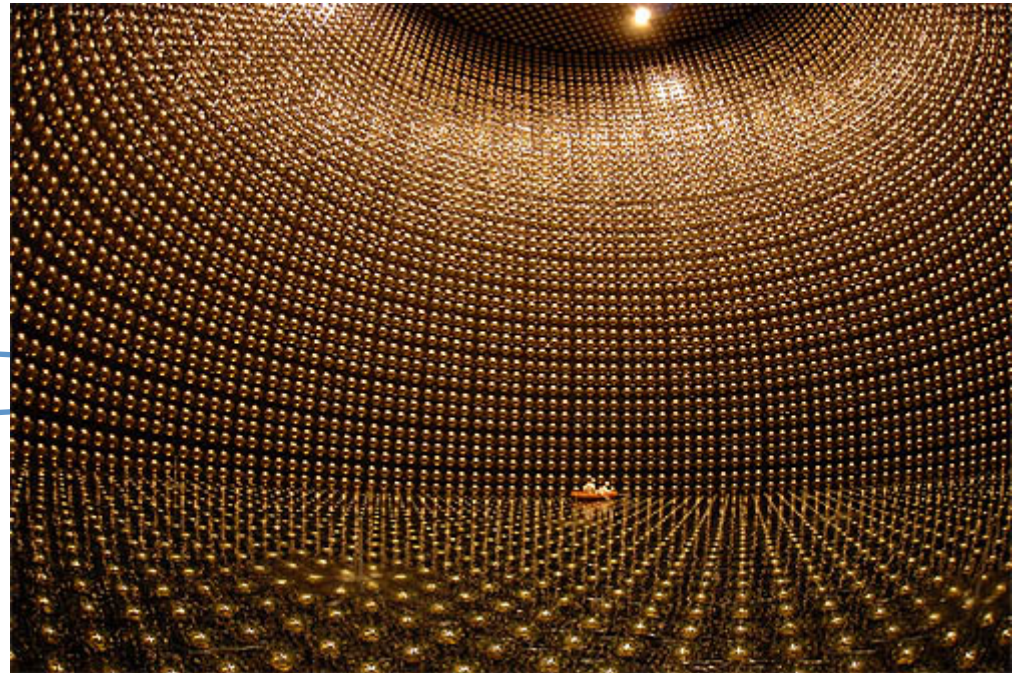
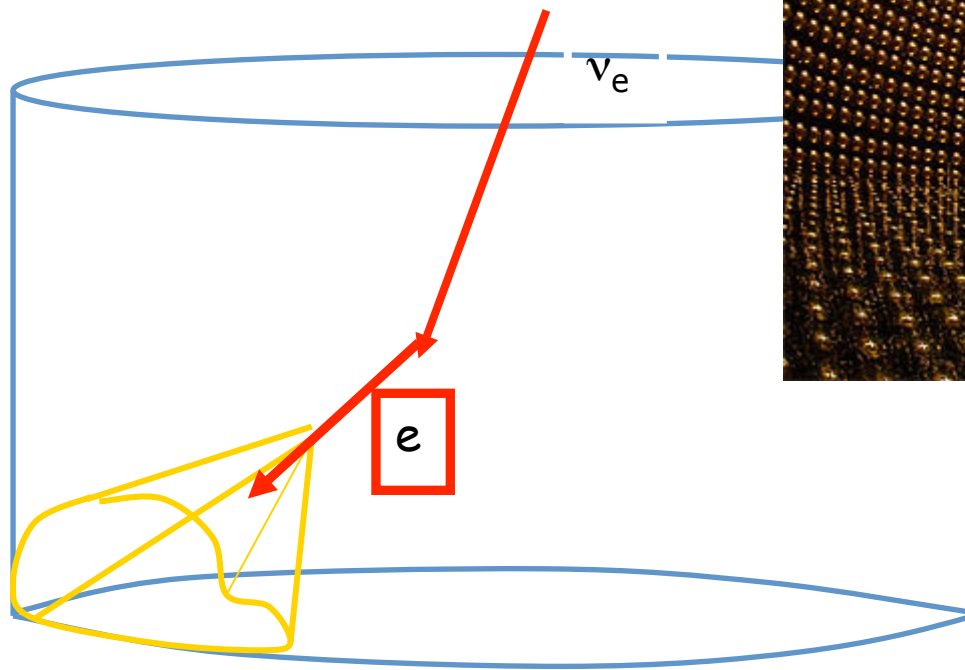


Astrofisica Nucleare e Subnucleare

Neutrino Detectors

The SK way- The elastic scattering of neutrinos on electrons

- Real-time detector
- Elastic scattering
 $\nu_e \rightarrow \nu_e$



Astrofisica Nucleare e Subnucleare

Cherenkov effect

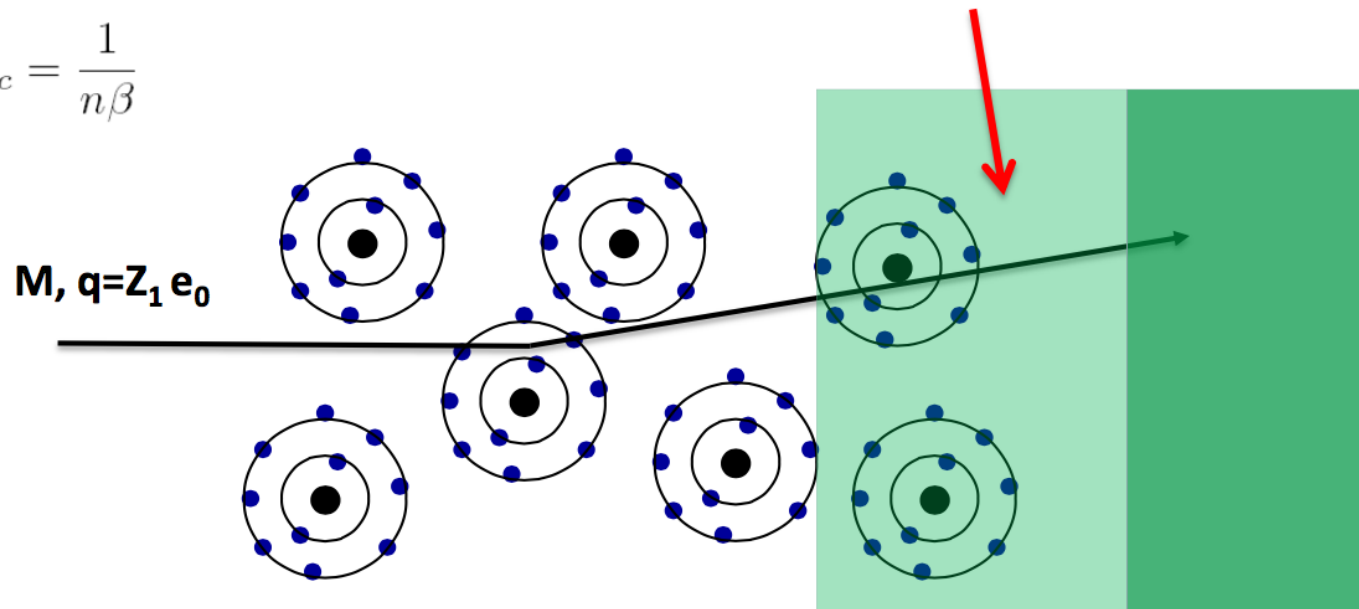
Cherenkov Radiation

If we describe the passage of a charged particle through material of dielectric permittivity ϵ (using Maxwell's equations) the differential energy cross section is >0 if the velocity of the particle is larger than the velocity of light in the medium

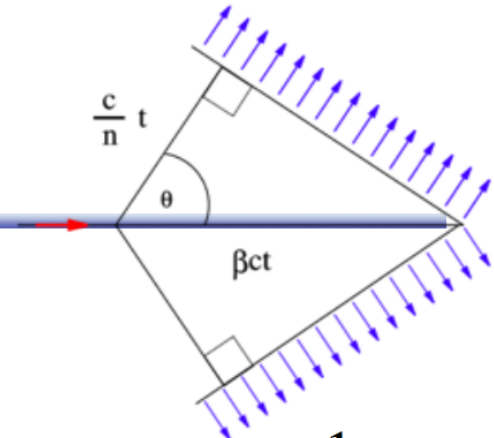
N is the number of Cherenkov Photons emitted per cm of material. The expression is in addition proportional to Z_1^2 of the incoming particle.

The radiation is emitted at the characteristic angle Θ_c , that is related to the refractive index n and the particle velocity by

$$\cos \Theta_c = \frac{1}{n\beta}$$



Cherenkov radiation



Velocity of the particle: v

Velocity of light in a medium of refractive index n : c/n

Threshold condition for Cherenkov light emission: $v_{th} \geq \frac{c}{n} \Rightarrow \beta_{th} \geq \frac{1}{n}$

$$-\left\langle \frac{dE}{dx} \right\rangle_{Cherenkov} \propto z^2 \sin^2 \theta_c$$

$$\cos \theta_c = \frac{1}{n\beta}$$

for water $\theta_c^{\max} = 42^\circ$

for neon at 1 atm $\theta_c^{\max} = 11 \text{ mrad}$

Energy loss by Cherenkov radiation very small w.r.t. ionization (< 1%)

Typically $O(1-2 \text{ keV / cm})$ or $O(200-1000)$ visible photons / cm

Visible photons:

$E = 1 - 5 \text{ eV}; \lambda = 300 - 600 \text{ nm}$

Cherenkov radiation

In a Cherenkov detector the produced photons are measured

Number of emitted photons per unit of length:

- wavelength dependence $\sim 1/\lambda^2$

$$\frac{d^2 N}{d\lambda dx} = \frac{2\pi\alpha z^2}{\lambda^2} \left(1 - \frac{1}{\beta^2 n^2(\lambda)}\right) = \frac{2\pi\alpha z^2}{\lambda^2} \sin^2 \theta_C$$

Integrate over sensitivity range:
[for typical Photomultiplier]

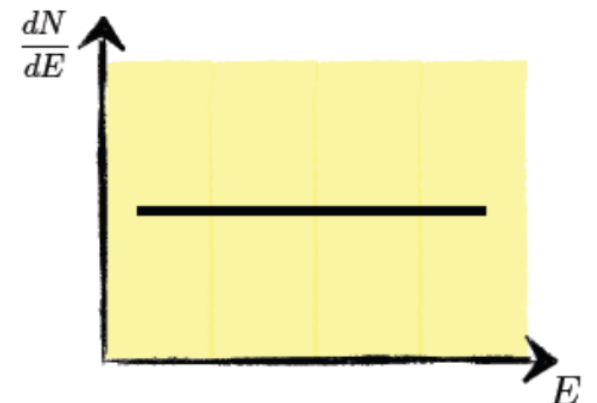
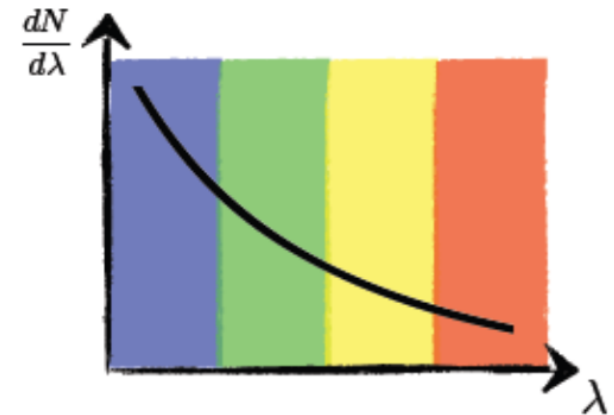
$$\frac{dN}{dx} = \int_{350 \text{ nm}}^{550 \text{ nm}} d\lambda \frac{d^2 N}{d\lambda dx}$$

$$= 475 z^2 \sin^2 \theta_C \text{ photons/cm}$$

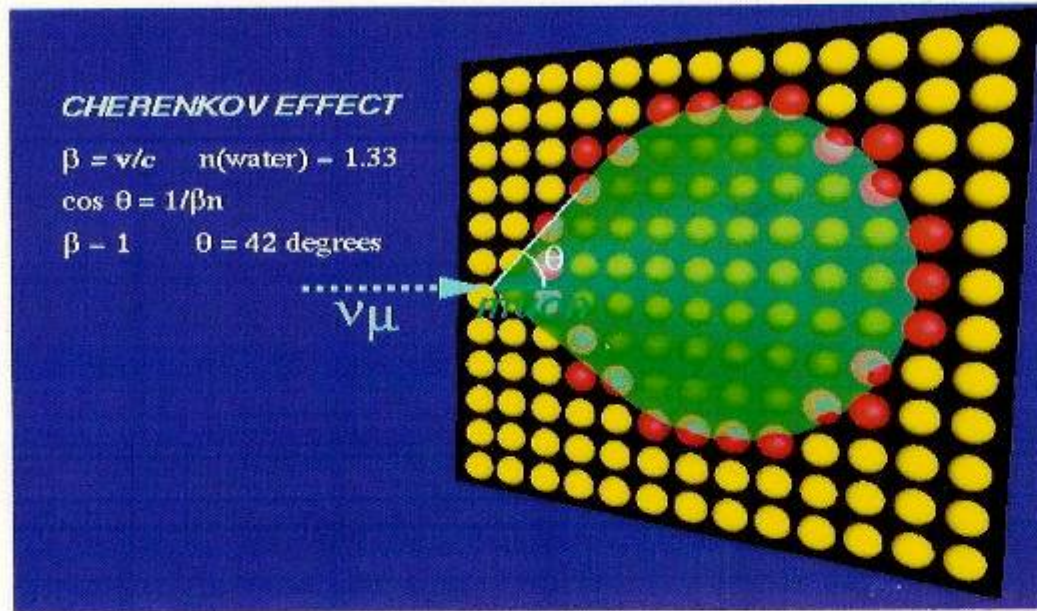
- energy dependence \sim constant

$$\frac{d^2 N}{dE dx} = \frac{z^2 \alpha}{\hbar c} \left(1 - \frac{1}{\beta^2 n^2(\lambda)}\right) = \frac{z^2 \alpha}{\hbar c} \sin^2 \theta_C$$

$$\frac{d^2 N}{dE dx} = 370 \sin^2 \theta_C \text{ eV}^{-1} \text{ cm}^{-1} \approx \text{const}$$



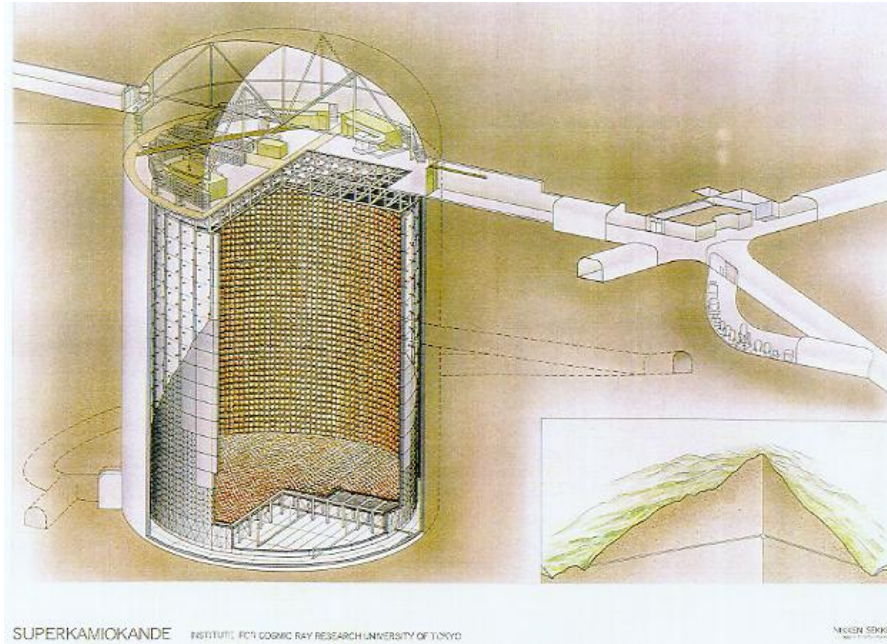
Cherenkov Radiation



One of the
13000 PMT



Neutrino Scattering Experiments - SuperKamiokande



- **Size: Cylinder of 41.4m (Height) x 39.3m (Diameter)**
- **Weight: 50,000 tons of pure water**
- **Light Sensitivity: 11,200 photomultiplier tubes
(50cm each in diameter -the biggest size in the world)**
- **Energy Resolution: 2.5% (at 1 GeV)
~16% (at 10 MeV)**
- **Energy Threshold 5 MeV**

Neutrino Scattering Experiments

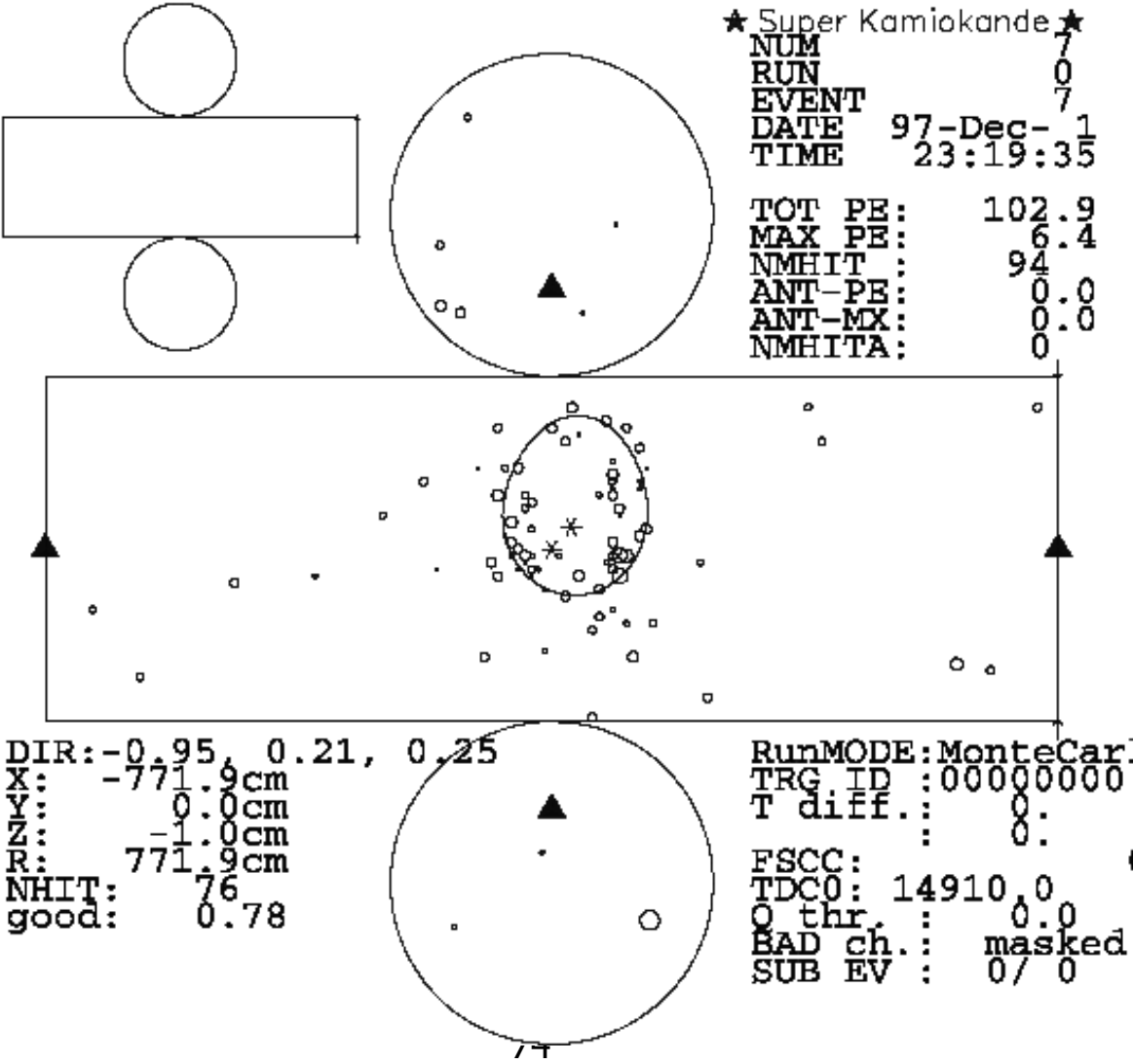
Particle	Cherenkov threshold in total Energy
e^{\pm}	0.768(MeV)
μ^{\pm}	158.7
π^{\pm}	209.7

Cherenkov threshold energies of various particles.

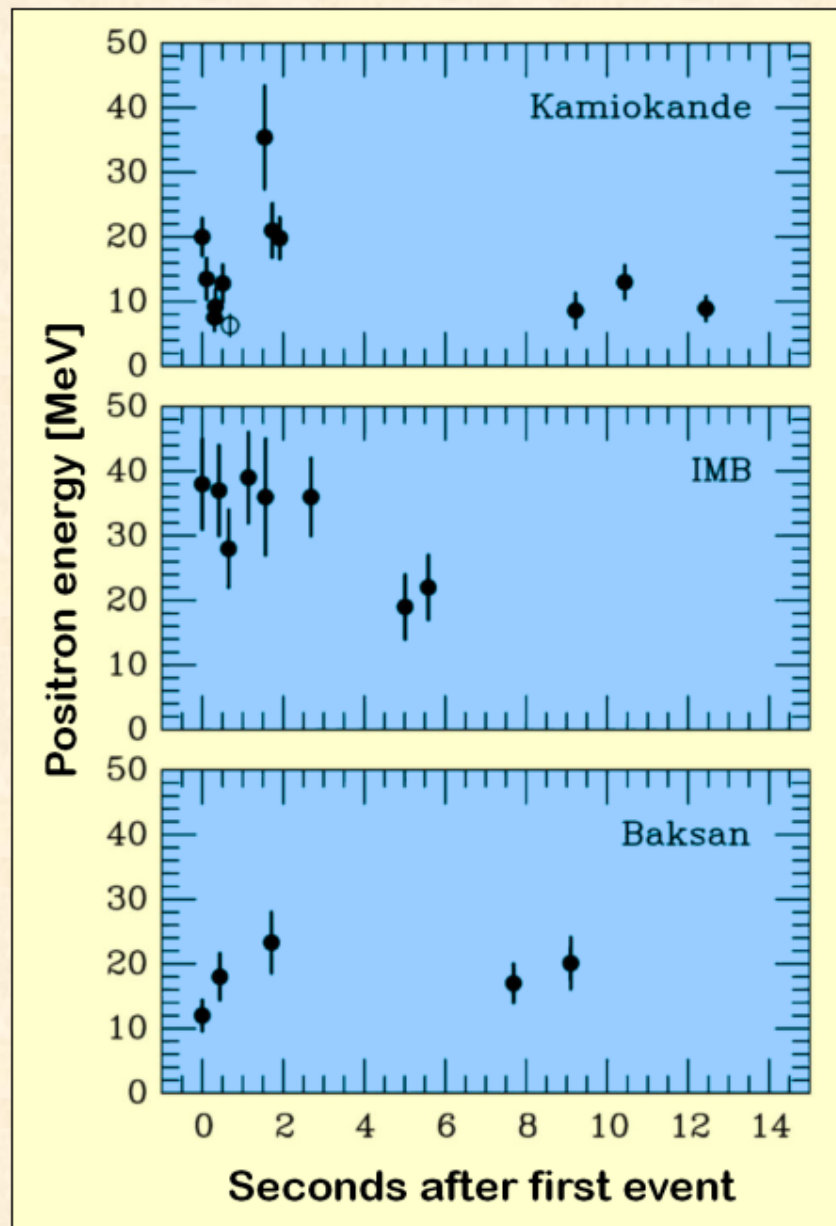
$$\cos \theta = \frac{1}{n\beta'}$$

Cherenkov light is emitted in a cone of half angle θ from the direction of the particle track

Neutrino Scattering Experiments



Neutrino Signal of Supernova 1987A



Kamiokande (Japan)
Water Cherenkov detector
Clock uncertainty ± 1 min

Irvine-Michigan-Brookhaven
(USA)
Water Cherenkov detector
Clock uncertainty ± 50 ms

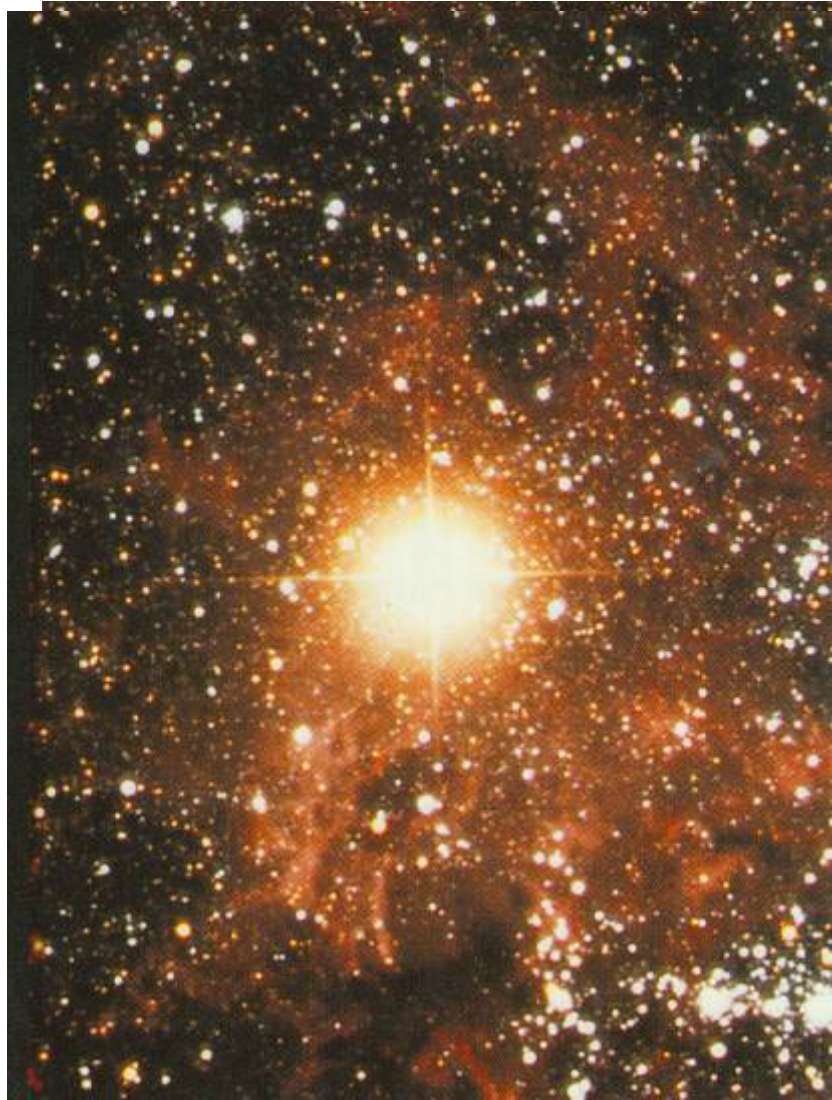
Baksan Scintillator Telescope
(Soviet Union)
Clock uncertainty $+2/-54$ s

Within clock uncertainties,
signals are contemporaneous

Astrofisica Nucleare e Subnucleare

Supernovae Neutrinos

Supernovae

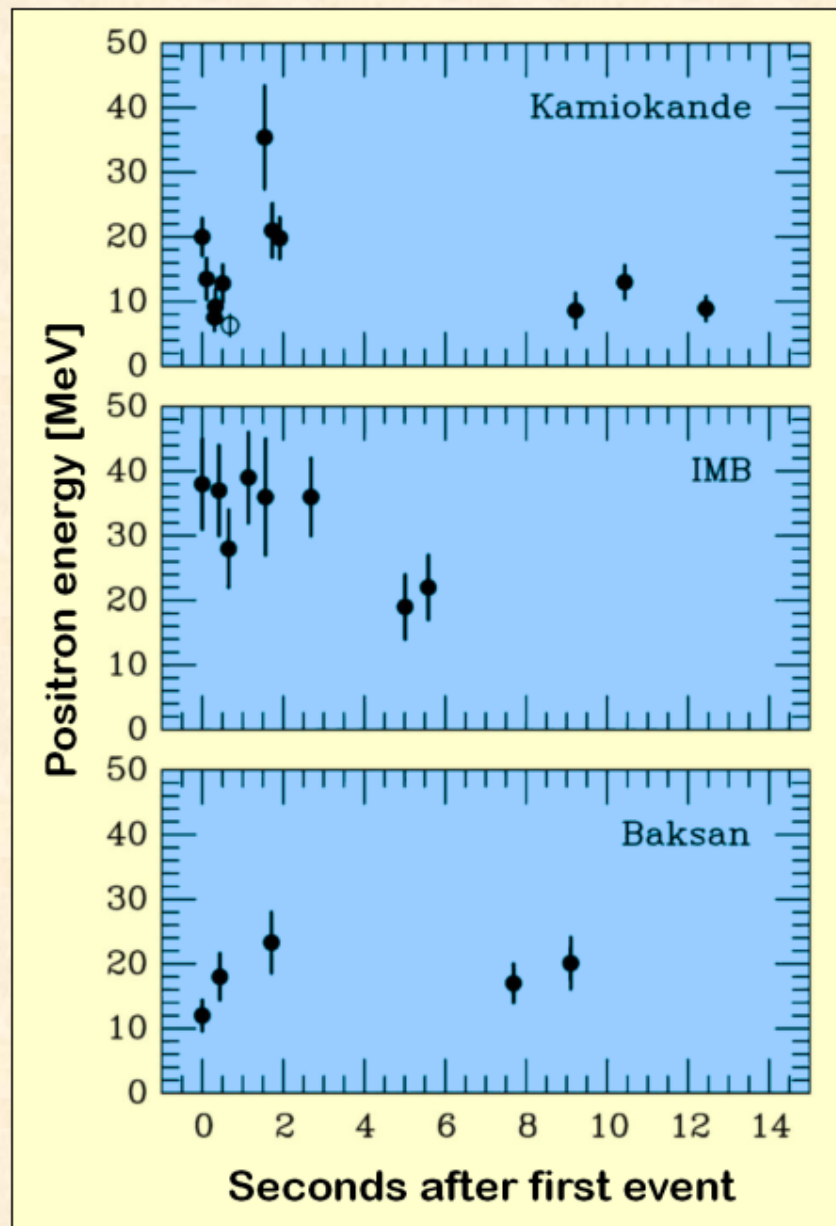


The field of the
supernova SN1987A
after 23 February 1987.

This picture shows a
small area of sky in the
Large Magellanic Cloud,
the nearby dwarf
companion galaxy to
our own Galaxy.

Anglo-Australian Telescope

Neutrino Signal of Supernova 1987A



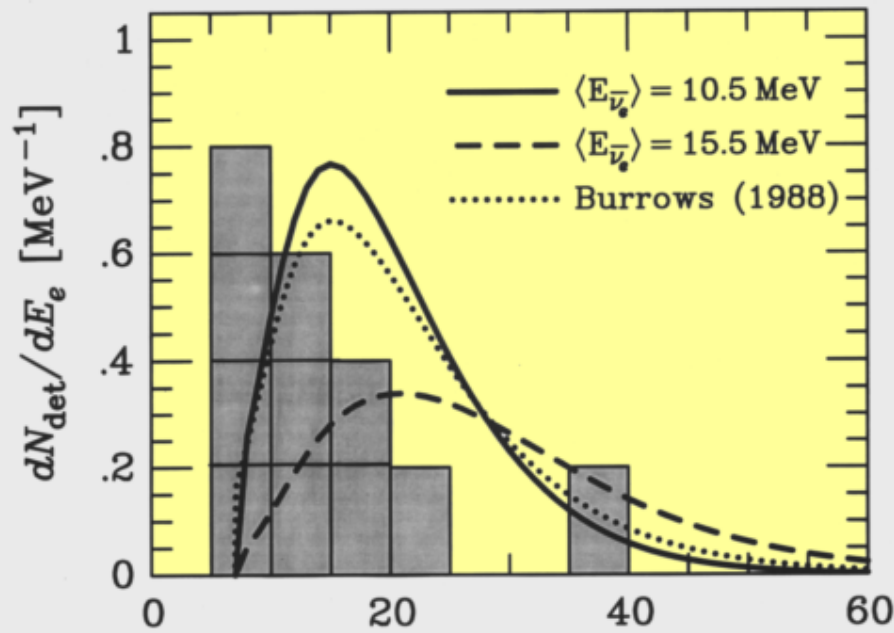
Kamiokande (Japan)
Water Cherenkov detector
Clock uncertainty ± 1 min

Irvine-Michigan-Brookhaven
(USA)
Water Cherenkov detector
Clock uncertainty ± 50 ms

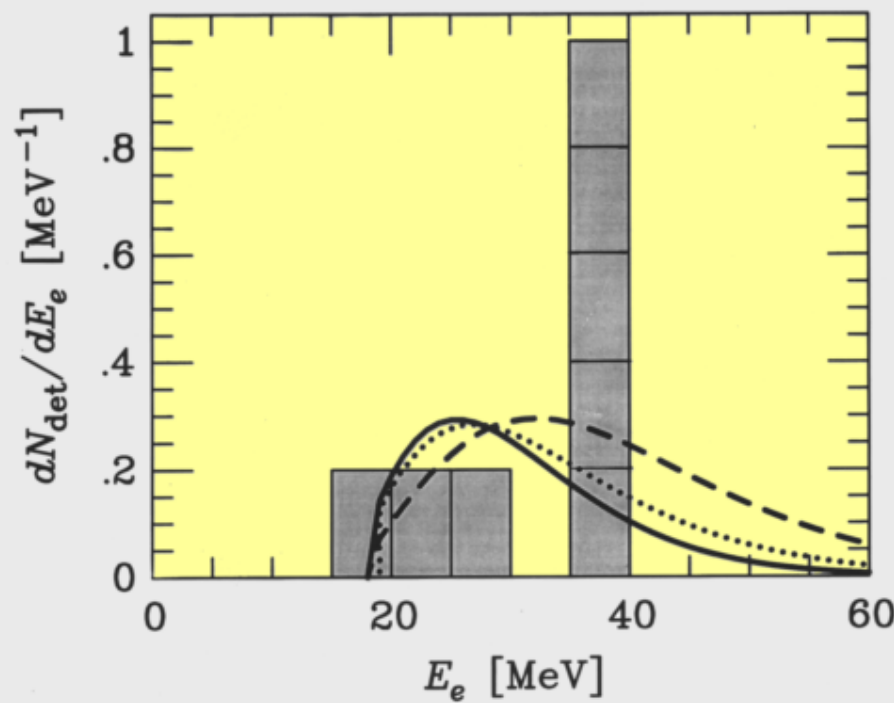
Baksan Scintillator Telescope
(Soviet Union)
Clock uncertainty $+2/-54$ s

Within clock uncertainties,
signals are contemporaneous

Energy Distribution of SN 1987A Neutrinos



Kamiokande II



IMB